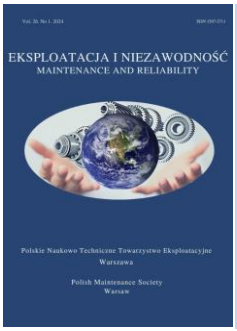

Eksploatacja i Niezawodnosc – Maintenance and Reliability

Volume 26 (2024), Issue 1

journal homepage: http://www.ein.org.pl

Article citation info:
Wang R, Jia X, Liu Z, Dong E, Li S, Cheng Z, Conditional generative adversarial network based data augmentation for fault diagnosis of diesel engines applied with infrared thermography and deep convolutional neural network, Eksploatacja i Niezawodnosc – Maintenance and Reliability 2024: 26(1) http://doi.org/10.17531/ein/175291

Conditional generative adversarial network based data augmentation for fault diagnosis of diesel engines applied with infrared thermography and deep convolutional neural network

Indexed by: Web of Science Group

Rongcai Wang[a], Xisheng Jia[a], Zichang Liu[a], Enzhi Dong[a], Siyu Li[a], Zhonghua Cheng[a,*]

[a] Shijiazhuang Campus, Army Engineering University of PLA, China

Highlights

- Utilize infrared thermography and deep convolutional neural network (DCNN) for fault diagnosis of diesel engines.
- Conditional generative adversarial network is deployed for data augmentation of the diesel engine infrared images.
- DCNN-based fault diagnosis method has better classification effect and algorithm stability compared with stacked auto-encoder, long short-term memory network and multi-layer perceptron.

Abstract

This paper tries to introduce a new intelligent method for the early fault diagnosis of diesel engines. Firstly, infrared thermography (IRT) is introduced into diesel engine condition monitoring, then infrared images of diesel engines in four health states, such as normal condition, single-cylinder misfire, multi-cylinder misfire and air filter blockage, are collected and the region of interest (ROI) of infrared images are extracted. Next, conditional generative adversarial network (CGAN) is deployed to perform data augmentation on infrared image datasets. Then, deep convolutional neural network (DCNN) and Softmax regression (SR) classifier are used for automatically extracting infrared image fault features and pattern recognition, respectively. Finally, a comparison with three deep learning (DL) models is performed. The validation results show that the data augmentation method proposed in the paper can significantly improve the early fault diagnosis accuracy, and DCNN has the best fault diagnosis effect and resistance to temperature fluctuation interference among the four DL models.

Keywords
diesel engines, data augmentation, conditional generative adversarial network, infrared thermography, deep convolutional neural network, fault diagnosis

This is an open access article under the CC BY license (https://creativecommons.org/licenses/by/4.0/)

1. Introduction

Diesel engine is the core power unit of many production systems, including construction machinery, agricultural vehicles, electric generators, ships, etc. Its working condition determines the reliability and overall efficiency of the system [12]. Due to the complex working environment and certain inherent manufacturing process defects, diesel engines are prone to various early faults during high temperature and pressure, high speed and heavy load operation, which can seriously affect productivity or even cause major safety accidents [14]. Therefore, to maintain the safety and stable operation of diesel engines, it is crucial to implement effective and reliable monitoring and diagnosis of diesel engine early faults and to take necessary maintenance measures.

To solve this problem, various sensor signals are applied for fault diagnosis of diesel engines, mainly including vibration signals, sound signals, oil signals, pressure signals and speed-

(*) Corresponding author.
E-mail addresses: R. Wang (ORCID: 0000-0001-6839-1181) wrcpromising@163.com, X. Jia asd3v36@163.com, Z. Liu zc_liu1997@aeu.edu.cn, E. Dong ez_dong@aeu.edu.cn, S. Li sy_li1988@163.com, Z. Cheng a15032073178@sina.com

torque signals [53]. Among the above signal analysis methods, vibration signals are easy to measure and contain important dynamic information of related mechanical components, such as the burst combustion of gases in the engine cylinder, the impact of valves during opening and seating, the reciprocating inertial impact of pistons, and crankshaft rotation, etc. [54, 5], which have been widely used in fault diagnosis studies of diesel engines [2, 8, 43]. However, vibration signal detection and acquisition has some prominent limitations, including noise pollution, local contact measurement, and high computing costs, etc. Furthermore, the acquisition environment of diesel engine vibration signals is usually a high temperature and violently vibrating cylinder surface, which can easily lead to distorted or even damaged sensor measurements [51]. Besides, in many industrial production activities, vibration signal acceleration sensors are not allowed to be deployed [55]. Due to the above reasons, the development of alternative sensor technologies for monitoring the health state of diesel engines has become a hot research topic.

In recent years, using contact sensors such as thermistors and thermocouples to collect temperature signals to carry out condition monitoring of mechanical equipment has attracted wide attention of researchers [26]. Common fault patterns of diesel engines such as misfire, air filter blockage, and insufficient oil supply are usually accompanied by significant temperature changes on the cylinder surface. However, contact temperature measurement usually only collects temperature changes at a few points on the equipment surface, which cannot fully characterize the real-time status of diesel engines. On this basis, infrared thermography (IRT) has gradually become a new non-contact nondestructive testing technique for measuring the surface temperature of equipment to overcome the negative effects of complex transmission paths and local detection caused by the contact temperature measurement. Compared with traditional methods based on vibration signal analysis, IRT-based fault diagnosis methods have the following outstanding advantages: 1) As the core device of the IRT system, infrared thermal camera can monitor the surface temperature of the equipment under test without contacting it and visualize it through infrared images; 2) IRT can detect the equipment remotely and in a wide range, which is suitable for health state monitoring of large mechanical equipment. 3) Unlike the vibration signal analysis method, IRT-based method is not affected by the vibration frequency of mechanical equipment. In summary, infrared images reflect the temperature changes of the equipment and the surrounding environment, and contain rich information about the equipment state, which can be well applied to the subsequent fault diagnosis studies. Other non-contact detection techniques, such as sound signal detection, have some shortcomings such as low signal-to-noise ratio and complex noise pollution, and traditional signal processing methods are difficult to separate and extract the fault signals. Therefore, IRT-based fault diagnosis methods for mechanical equipment have been widely studied and applied by scholars at home and abroad [42, 16, 39]. However, the existing IRT-based fault diagnosis methods have the following main challenges in the practical industrial applications of mechanical equipment:

(1) Currently, IRT-based fault diagnosis methods of mechanical equipment usually require manual extraction of infrared image feature parameters, and the process of feature selection requires a large amount of a priori knowledge, but in actual industrial applications, such a priori knowledge is not always available in time, which largely affects the accuracy of fault diagnosis;

(2) During the operation of mechanical equipment, the surface temperature usually changes according to the rule of first increasing and then remaining stable, but the fault may occur at any time after the power is turned on. The current IRT-based methods mostly collect infrared images of the equipment in the stable state and carry out fault diagnosis afterwards, without considering the influence of temperature changes on the fault diagnosis results at the early stage of equipment operation;

(3) To date, IRT has been widely used for fault pattern identification of rotating machinery such as rolling bearings, rotor systems, and shafts in steady state, but there is a lack of diagnostic research for early faults of mechanical equipment, especially a lack of research on early fault identification of reciprocating machinery such as diesel engines based on IRT.

For early faults of diesel engines, especially minor faults, there is often a lack of supervision signals with obvious labels and sufficient training samples. In this case, the method of unsupervised learning [32, 46, 50] can play an important role. Unsupervised learning can learn useful structures and patterns from input data without labels or supervision signals. Through

the data augmentation technology based on unsupervised learning, simulated synthetic data with early fault characteristics can be generated, which can be used to train and optimize the diagnosis model and improve the early fault detection ability of the model.

Therefore, to make up for the above research deficiencies, a new unsupervised data augmentation based fault diagnosis method is proposed for the problems of inconspicuous infrared image features and insufficient training data at the early stage of diesel engine operation, which can achieve accurate and efficient diagnosis of early faults of diesel engines with the unique advantages of IRT. Firstly, infrared images of diesel engines in different health states are obtained by using infrared thermal camera detection, followed by data augmentation of the experimental dataset with conditional generative adversarial network (CGAN), then feature parameters of infrared images are automatically extracted based on deep convolutional neural network (DCNN), and finally Softmax regression (SR) classifier is deployed for fault pattern recognition of diesel engines, while the experimental data collected from a high-pressure common rail diesel engine is used to verify the effectiveness of the proposed method.

The remainder of the paper is organized as follows: Section 2 reviews and analyzes the related literature and the current status of research. In Sections 3 and 4, the basic principles and methodological procedures of CGAN and DCNN are introduced, respectively. Section 5 details the basic components of the fault diagnosis system of diesel engines and information about the infrared image acquisition experiment, and analyzes the CGAN-based data augmentation process. In Section 5, the effectiveness and superiority of the proposed method are verified using the experimentally obtained datasets. Finally, Section 7 summarizes the innovative work of the paper.

2. Related literature review

IRT-based fault diagnosis of mechanical equipment mainly includes three steps: infrared image acquisition, feature parameter extraction and fault pattern recognition. Among them, feature parameter extraction is the most critical step among the above steps [24], which directly affects the accuracy of subsequent pattern recognition. In recent years, deep learning (DL) has received key attention from all walks of life for its excellent feature extraction ability, and has been widely applied in speech recognition, image processing, machine vision and other fields [21, 33, 28, 35]. Compared with the traditional method of manually extracting feature parameters, DL can directly process a large amount of raw data, dig deep into the intrinsic laws of data, and carry out adaptive learning of mapping relationships between data without artificially establishing complex mathematical models, which effectively reduces the information loss brought by manual processing. Furthermore, in the context of big data, DL can effectively improve the intelligence and adaptability of fault diagnosis. Based on the excellent feature extraction ability of DL, many researchers are working on the application of DL methods in the field of fault diagnosis of mechanical equipment [13, 38, 17].

Verstraete et al. [41] addressed the shortcomings of traditional manual feature extraction methods, such as complicated operation and the need for more expert knowledge of the relevant system, by converting the original data into time-frequency images and then inputting them into DCNN for adaptive feature extraction and fault diagnosis, which can overcome the uncertainty brought by insufficient expert knowledge to the diagnosis results. Jia et al. [18] introduced IRT into fault diagnosis of bearings to solve the problems of rotating machinery damage and noise pollution caused by sensor installation in the process of vibration signal acquisition, and the feature extraction and fault diagnosis effects of bag of visual words (BoVW) and convolutional neural network (CNN) were compared and analyzed. Liu et al. [27] proposed a fault diagnosis method of the rolling bearing based on sound signal analysis, which uses short-time Fourier transform (STFT) to convert the acoustic signal into a spectrogram and input it into a stacked sparse self-encoder (SSAE) network for adaptive extraction of fault features, and finally SR classifier is deployed for fault pattern recognition. Xiao et al. [48] proposed a fault diagnosis model of the insulator string based on IRT and probabilistic neural network (PNN) for the close relationship between insulator string state and its surface temperature distribution, and the automatic identification of fault patterns can be achieved by using the SR classifier. Xu et al. [49] addressed the limitations of existing methods in feature learning, converted the one-dimensional vibration signal into a two-dimensional grayscale image based on continuous wavelet

transform (CWT), and used DCNN and random forest (RF) integrated learning method for fault diagnosis research of bearings, and the experimental results demonstrated that the method has a high accuracy.

The combination of IRT and DL has also seen some research progress. Choudhary [4] et al. collected infrared images of rolling bearings in six different states, and used artificial neural networks (ANN) and LeNet-5 for feature extraction and pattern recognition, and demonstrated the superiority of CNN by comparing and analyzing the classification results of the two methods. Li et al. [26, 25] achieved good results in an in-depth study of failure patterns in industrial gearboxes and rotor systems, using IRT and CNN for infrared image acquisition and pattern recognition of common faults. Wang [44] et al. proposed a crack recognition method based on IRT with CNN for image recognition and classification to address the problems of low efficiency and poor interference resistance in steel plate crack detection by traditional non-destructive testing (NDT) techniques, and achieved high recognition accuracy on the test set.

In summary, we can see that DL methods have better fault diagnosis performance compared to traditional methods that rely on manually designed features. Currently, the common methods and basic processes for fault diagnosis of diesel engines are mainly signal acquisition, manual feature extraction, and pattern recognition based on machine learning (ML). Under this research theme, Ramteke et al. [34] used fast Fourier transform (FFT) and STFT to extract feature parameters from the collected vibration and sound signals of diesel engines in different wear states and ANN is applied for failure pattern identification. Flett et al. [9] proposed a fault diagnosis method for valve train of the diesel engine based on a Naive Bayes Classifier, which can achieve accurate identification of fault patterns such as valve spring deformation and abnormal clearance by improving the root mean square (RMS). Kowalski et al. [19] proposed a new fault diagnosis method based on the extreme learning machine (ELM) for 15 different health states of impulse program diesel engines.

In the research of IRT-based fault diagnosis of diesel engines, some scholars have started their preliminary exploration. Baranitharan et al. [1] proposed an intelligent life monitoring method for diesel engines based on infrared image processing technique, which quantifies the infrared images of engine operation using image processing techniques to assess the engine life in terms of pixel values. Li et al. [36] designed a test rig for monitoring diesel engine exhaust faults using IRT to measure the radiated temperature of the outer surface of the exhaust pipe under different operating conditions, and analyzed the relationship between diesel engine exhaust temperature and faults according to the principle of infrared thermometry. Using ultrasonic IRT, Su et al. [37] carried out ultrasonic IRT principle and series of experimental studies for the limitations of traditional NDT technology in detecting crack defects in aero-engine blades, and built an ultrasonic IRT detection test platform to achieve the detection of fine cracks in aero-engine guide blades and working blades.

Although some achievements have been made in the research of diesel engine fault diagnosis, there are still many deficiencies in the application of traditional ML, including the cumbersome feature engineering, the need for manual intervention, the inability to automatically learn, and the limited ability to process large-scale nonlinear data. CNN has been proven to be an effective method in the field of feature extraction [29, 10]. Compared with traditional ML methods, CNN has two significant advantages: 1) It can automatically extract deep level features of data and has good generalization ability; 2) By using local connections and weight sharing, the network parameters are easy to train and optimize [47]. DCNN has a more complex network structure and better feature extraction ability compared to general CNN models. Therefore, in this study, DCNN was used to extract infrared image feature parameters of diesel engines under different fault patterns.

From the above literature, it can be seen that the methods based on IRT and DL are widely used in the field of rotating machinery fault diagnosis, however, the acquisition process of infrared images is usually carried out in the stable state after the equipment has been running for a period of time, and the research of early fault diagnosis for rotating machinery under variable temperature still needs to be explored; for reciprocating machinery such as diesel engines, the research of fault diagnosis based on IRT and DL is in the initial stage, and the early fault diagnosis research of diesel engines under variable temperature is still a blank.

To fill the above research gaps, this paper simulates several

common fault patterns and collects infrared images under different fault states using a diesel engine experiment bench for the variable temperature process from start-up operation to temperature stabilization, and then CGAN and DCNN are applied for data augmentation and infrared image fault feature extraction for early fault diagnosis of the diesel engine. The infrared image dataset is divided into several sub-datasets according to the same time interval and used to verify the effect of temperature variation on the accuracy and stability of the algorithm.

3. CGAN-based data augmentation

In the application of DL methods, only limited data can be acquired for model training in many cases, so data augmentation operation is an indispensable part. Data augmentation methods mainly include two categories of supervised data augmentation and unsupervised data augmentation methods, which are classified as shown in Figure 1.

In recent years, with the continuous development of DL techniques, unsupervised data augmentation methods have received more and more attention. For example, generative adversarial network (GAN) [11] has been widely used in many fields such as image processing, speech processing, computer vision (CV), and natural language processing (NLP), including image generation [40], style migration [15], super-resolution [6], and image restoration [7]. As an unsupervised generative DL model, GAN adopts the idea of confrontation optimization in its structural design. Among the many functions of GAN, image generation is the most widely used, aiming to generate the desired images using the generator.

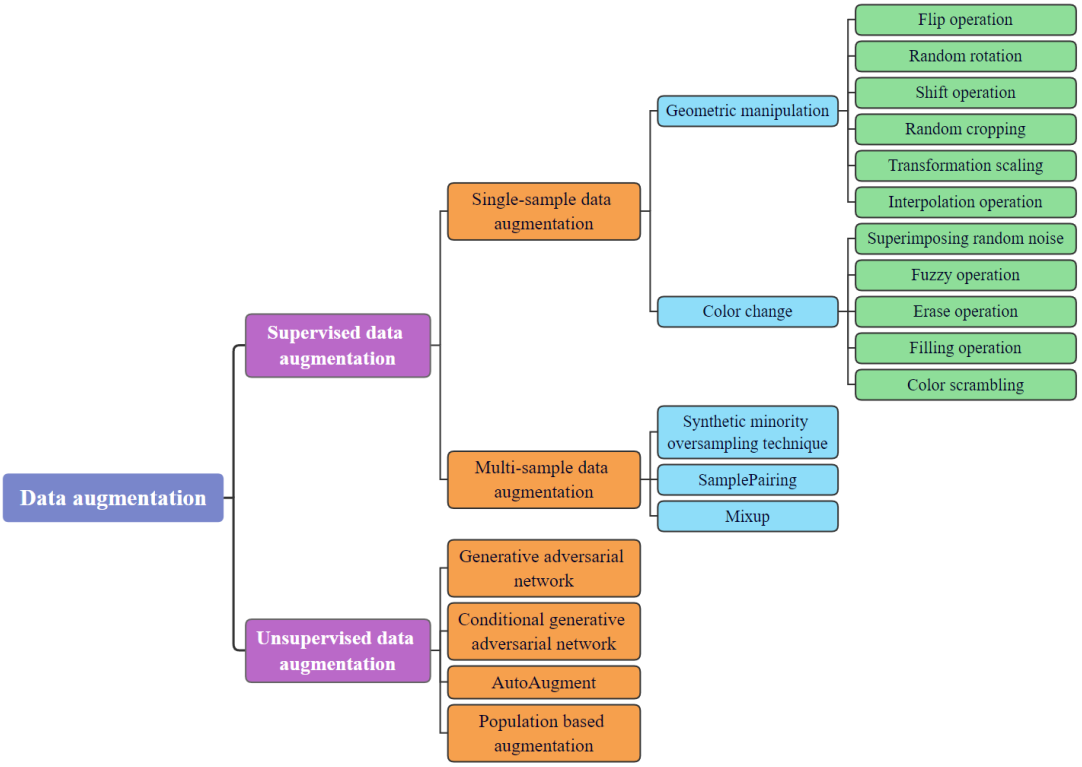

Fig. 1. Classification of data augmentation methods.

3.1. The network structure of CGAN

GAN consists of two neural network models, a generator G and a discriminator D. The role of the generator is to generate virtual data similar to the real data by inputting random noise, while the role of the discriminator is to determine whether the input data is real or virtual. The iterative training of GAN is the process of continuous adversarial optimization of the generator and the discriminator, and the performance of both the generator and the discriminator can be effectively improved so that the virtual data generated by the generator cannot be distinguished by the discriminator, thus achieving the purpose of image generation. The training of GAN can be stopped when the quality of the output samples of the generator no longer improves, i.e., the discriminator is unable to determine the authenticity of the data generated by the generator. The method flow of GAN is shown in Figure 2 [23].

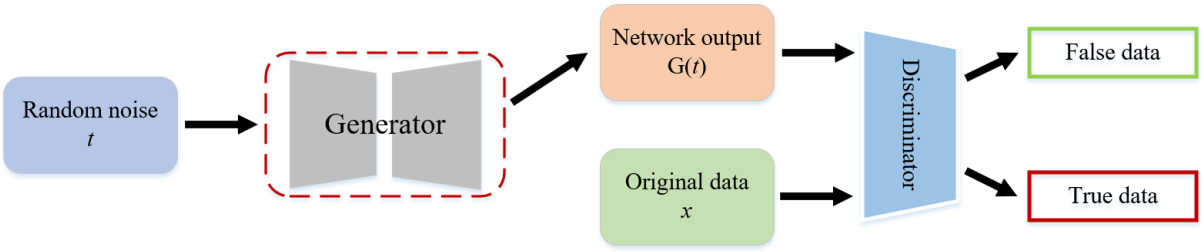

Fig. 2. The method flow of GAN.

CGAN has made some improvements on the basis of GAN. For the generator of the original GAN, the generated images are random and unpredictable, so the output of the network cannot be controlled, and the actual operability is not strong. In response to the issue of the inability of the original GAN to generate images with specific attributes mentioned above, Mehdi Mirza et al. [30] proposed CGAN in 2014, which generates images that meet specific conditions by adding constraints to the generator and discriminator in the original GAN. The method flow of CGAN is shown in Figure 3.

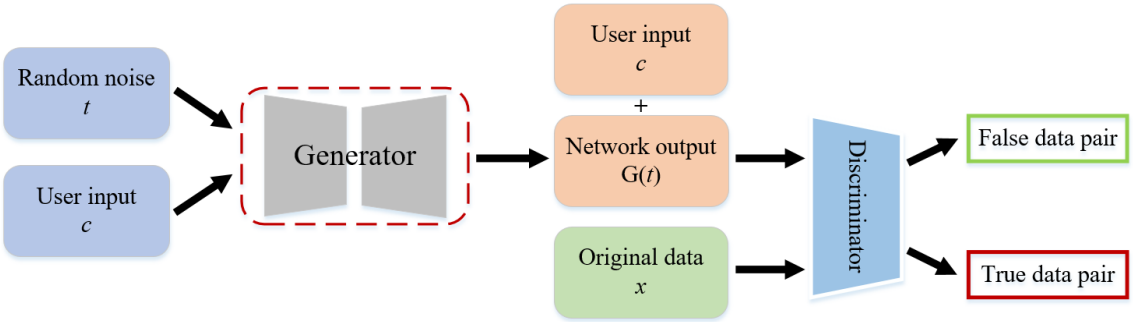

Fig. 3. The method flow of CGAN.

CGAN is a generative model that learns how to generate images from random noise corresponding to given conditions by means of adversarial training, so that the generated images have the same distribution as the original images, thus achieving the task of image generation.

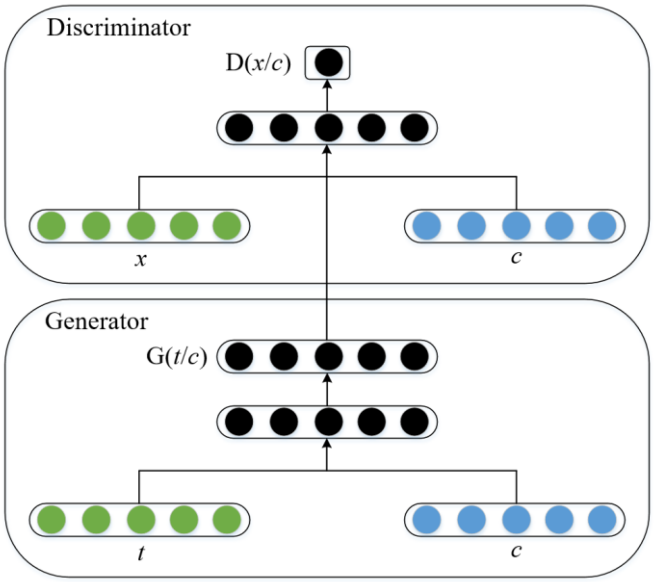

Fig. 4. The network structure of CGAN.

CGAN essentially incorporates additional added constraints into the generator G and discriminator D, which can be in any form, such as text, labels, images etc., aiming to enable the network to be better trained under the corresponding requirements. Except for the introduction of conditional constraints, the implementation process of CGAN is basically the same as that of GAN. The network structure of CGAN is shown in Figure 4.

As can be seen in Figure 4, the constraint c is introduced as additional input information to CGAN, which is combined with the random noise t as the input to the generator G; while in the discriminator D, the constraint c and the output of the generator are combined with the original data x as the input to the discriminator. This improvement has been shown to be very effective in many studies [31, 3, 45].

3.2. The loss function of CGAN

During the iterative training of GAN and its modified forms, the adversarial optimization between the generator and discriminator can be viewed as a maximal and minimal game,

where the generator tries to maximize the error rate of the discriminator and the discriminator tries to minimize its error rate. This competition drives the training of the model and motivates the generator to generate more realistic data and the discriminator to become more accurate. The loss function of a classical GAN is as follows [11]:

$$V(G,D) = E_{x\sim p_{data(x)}}[log\, D\,(x)] + E_{t\sim p_{t(t)}}[log(\,1 - D(G(t)))] \quad (1)$$

where, x denotes the original data, t denotes the random noise input to the generator, $G(t)$ is the data generated by the generator, $D(x)$ is the probability that the discriminator judges the original data to be true, $D(G(t))$ denotes the probability that the discriminator judges the data generated by the generator to be true, and E represents the mathematical expectation under the specified data distribution of the solution. In summary, in the actual training process, GAN achieves the optimization of two models by alternating iterations. First, the generator is kept constant and the parameters of the discriminator are optimized so that it can better distinguish the real image from the generated image. Then, the discriminator is fixed and parameters of the generator are optimized so that it can generate more realistic images to deceive the discriminator. This process continues until a predetermined number of training sessions is reached or the quality of the generated images meets the requirements.

For the discriminator, where x is the original data, i.e., the real data, the optimization objective of its training process is to maximize the loss function $V(G,D)$, in other words, it is necessary to make $D(x)$ as large as possible while $D(G(t))$ is as small as possible, and the process of optimizing the discriminator can be expressed as follows:

$$\max_{D} V(G,D) = E_{x\sim p_{data(x)}}[log\, D\,(x)] + E_{t\sim p_{t(t)}}[log(1 - D(G(t)))] \quad (2)$$

For the generator, the optimization objective of its training process is to minimize the loss function $V(G,D)$, and the process of optimizing the generator with optimal discriminator parameters can be expressed as follows:

$$\min_{G} V(G,D) = E_{t\sim p_{t(t)}}[log(\,1 - D(G(t)))] \quad (3)$$

Therefore, the objective function of GAN can be represented by the following equation:

$$F_1 = \min_{G}\max_{D} V(G,D) \quad (4)$$

Except for the introduction of relevant conditional constraints, the implementation process and network structure of CGAN and GAN are basically the same. In the training process of CGAN, the constraints c are added to the inputs of both the generator and the discriminator, and then the loss function and objective function of CGAN are shown in Eq. (5) and Eq. (6), respectively [49].

$$V^*(G,D) = E_{x\sim p_{data(x)}}[log\, D\,(x/c)] + E_{t\sim p_{t(t)}}[log(\,1 - D(G(t/c)))] \quad (5)$$

$$F_2 = \min_{G}\max_{D} V^*(G,D) \quad (6)$$

where, $D(x/c)$ denotes the probability that the original data x is true after inputting both the constraints c and the original data x to the discriminator, and $D(G(t/c))$ represents the probability that the false data generated by the discriminator after inputting both the constraints c and the random noise t to the generator is judged to be true.

In summary, CGAN improves the quality and controllability of image generation by introducing constraints as user input, which is a simple and effective improvement on the classical GAN.

Diesel engines have a wide variety of fault types and fault degrees, and the data distribution corresponding to each fault type also has its own uniqueness. Using CGAN can simulate the signal data of various fault types, which greatly expands the source of training data. This can not only effectively improve the generalization ability of the model, but also help the model to better understand and learn the data distribution of various fault types. Moreover, CGAN-based data augmentation can also help to improve the real-time performance of the diagnosis model. Since CGAN can generate a large number of simulated data in the training process, it can greatly reduce the amount of real data needed for online diagnosis. In this way, the complexity of online calculation can be reduced, and the real-time diagnosis can be improved. CGAN-based data augmentation can not only improve the early fault diagnosis ability, generalization ability and robustness of the model, but also improve the real-time performance of the model, which has important application prospects.

4. DCNN-based feature extraction

CNN is a kind of feedforward neural network containing convolution computation for processing data with grid structure (e.g., images) proposed by Professor LeCun based on the idea of back propagation training delayed neural networks [20]. Meanwhile, DCNN usually contains multiple convolutional

layers, pooling layers and fully connected layers, which can better capture the high-level features of images and perform very well in many tasks such as image classification, target detection, speech recognition, natural language processing, etc. The structure of DCNN network is shown in Figure 5.

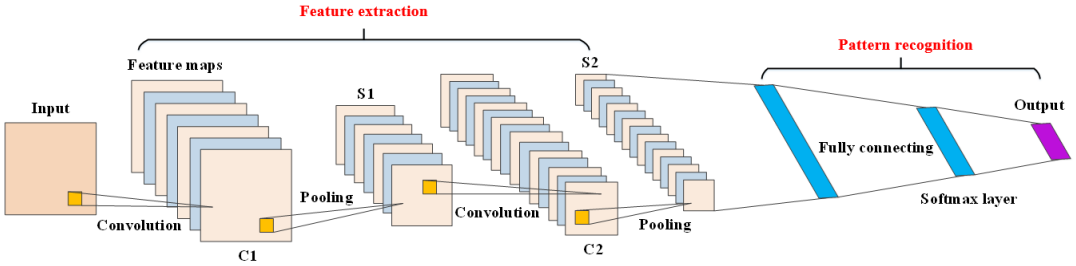

Fig. 5. Typical DCNN architecture.

4.1. Convolutional layer

The convolutional layer, as the core of DCNN, mainly uses a series of convolutional kernels to perform convolution operations on the input image data and output the feature map. Each convolutional kernel in the convolutional layer shares the same weight parameters, thus reducing the number of parameters of the whole model, alleviating the problem of overfitting, and also improving the generalization ability of the model. At the same time, the convolutional kernels convolve only local regions of the input image, thus preserving the local spatial information of the input image and making the model invariant to operations such as deformation and translation of the input image. The convolution operation can be described as follows:

$$\mathbf{x}_i^n = \mathbf{c}_n * \mathbf{x}_i{}^{n-1} + \mathbf{b}_i^n \tag{7}$$

where, $\boldsymbol{x}_i^n$ represents the i-th output mapping of the n-th layer, and $\boldsymbol{x}_i{}^{n-1}$ represents the i-th output mapping of the (n-1)th layer. $\boldsymbol{c}_n$ is the convolution kernel of the n-th layer, the symbol "*" represents the convolution operation, and $\boldsymbol{b}_i^n$ is the bias vector.

4.2. Activation layer

Convolution operation is a linear operation, no matter how many convolutional layers are superimposed, the output is a linear combination of the inputs, when the network has limited ability to express features and cannot handle complex nonlinear problems. Therefore, a nonlinear activation function needs to be added after the convolutional layers in order to give the network nonlinear description capability. The activation layer is usually located after the convolutional layer of the DCNN and is used to perform nonlinear transformations on the input data to better extract features and enhance the expressiveness of the model. The choice of the activation function has a great influence on the performance of the neural network. The common activation functions are: sigmoid function, tanh function, ReLU function, etc. The curves of each function and its expressions are shown in Figure 6, where the solid line is the activation function and the dashed line is its derivative.

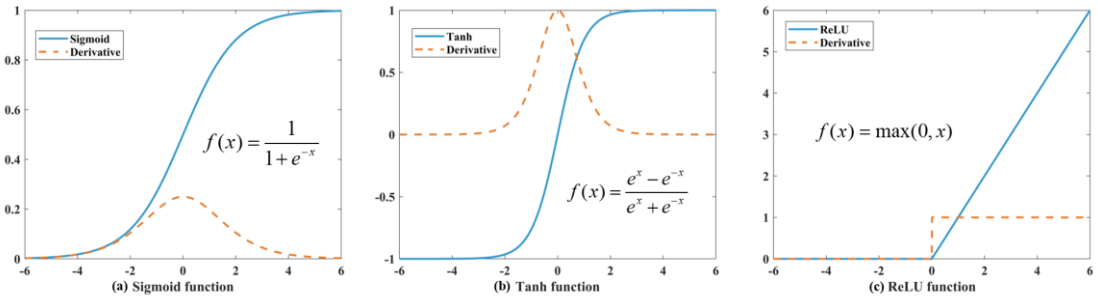

Fig. 6. Common activation functions.

Among the above three activation functions, ReLU function is the most widely used in CNN. Compared with the first two, ReLU function not only has faster convergence speed, but also has certain sparse expression characteristics of the output. Using one-sided inhibition can effectively avoid the gradient disappearance problem, which makes the training of neural networks more stable and has faster computation speed and better convergence.

4.3. Pooling Layer

The main role of pooling layer is to downsample the output of the convolution operation to obtain a smaller output feature map, thus reducing the number of parameters and computation of the network, while retaining the main feature information of the input. There are usually two types of pooling layers: maximal pooling and average pooling. Maximal pooling selects the largest value from each subregion of the input as the output. On the other hand, average pooling computes the average of each subregion as the output. A visual representation of the two pooling operations is shown in Figure 7.

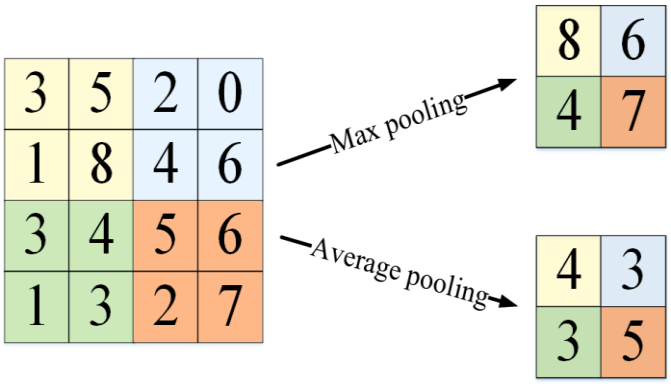

Fig. 7. Schematic diagram of two pooling operations.

In Figure 7, the size of the pooling kernel is 22. The pooling operation can be expressed by the following equation:

$$\mathbf{x}_i^n = down(\mathbf{x}_i^{n-1}) + \mathbf{b}_i^n \tag{8}$$

where, $\boldsymbol{x}_i^n$ denotes the i-th output mapping of the n-th layer, $down(\cdot)$ is the pooling function, and $\boldsymbol{b}_i^n$ represents the bias vector of the n-th layer.

The pooling layer can help the network learn a more robust feature representation and thus improve the generalization ability of the network. Since information about the location of a pattern or concept is usually encoded in the features, and the maximal value of the feature map region carries more information in terms of the amount of information compared to the average value, maximal pooling is used more often in the pooling process.

4.4. Fully connected layer

The fully connected layer is usually the last layer of DCNN, and its role is to flatten the feature maps (usually two-dimensional matrices) output from the convolutional and pooling layers into one-dimensional vectors, and to perform product and addition operations with a set of learnable weight matrices to obtain the final classification results by the SR classifier [22], as shown in Figure 8.

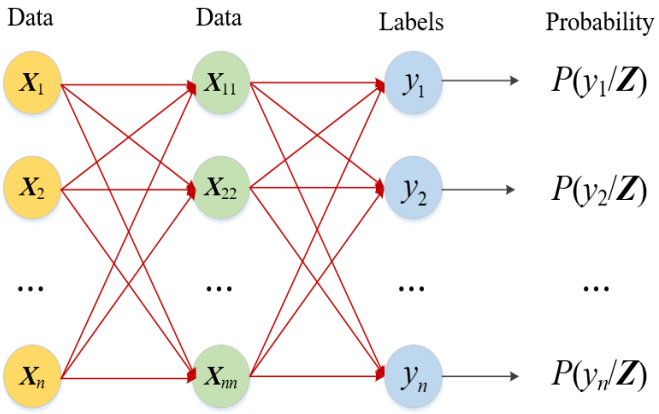

Fig. 8. Schematic diagram of the fully connected layer.

In Figure 8, $\boldsymbol{Z}$ represents the output of the final layer in the fully connected network for the sample to be classified, which usually contains the score of each class, i.e., the probability that the sample belongs to the corresponding class. Each neuron in the fully connected layer is connected to all the neurons in the previous layer, so the number of parameters in this layer is very large and it tends to lead to overfitting problems. To avoid this, some regularization operations, such as dropout or L2 regularization, are usually added before the fully connected layer.

5. The proposed system for fault diagnosis of diesel engines

In this paper, a fault diagnosis system of the diesel engine based on IRT and DCNN is proposed, including four basic modules such as infrared image acquisition, data augmentation, feature extraction, and pattern recognition, as shown in Figure 9. First, infrared images are acquired for different health states of the diesel engine, including four states of normal condition, single-cylinder misfire, multi-cylinder misfire, and air filter blockage; second, before extracting infrared image fault features, the region of interest (ROI) of the infrared image is extracted, and the CGAN-based infrared image generation method is applied for data augmentation processing; then, DCNN is deployed to automatically extract feature parameters of infrared images; finally, the fault features extracted in the previous step are divided into training and test sets according to a certain ratio, and the final pattern recognition is performed using the SR classifier.

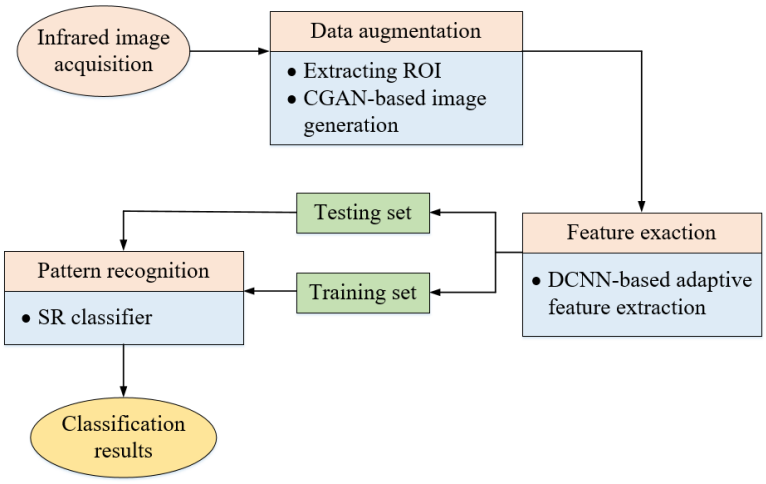

Fig. 9. Fault diagnosis system of the diesel engine.

It should be noted that the IRT-CGAN-DCNN based fault diagnosis method of the diesel engine does not require prior knowledge of equipment fault laws, parameter setting methods and other related priori knowledges when applied. It can directly collect infrared images of the diesel engine in different health states, which will be input to DCNN for fault pattern recognition through CGAN-based data augmentation processing. The method has excellent adaptive learning capability, simple and efficient application, and is highly adaptable to fault diagnosis of diesel engines. The specific process and visualization of the proposed fault diagnosis method of the diesel engine is shown in Figure 10.

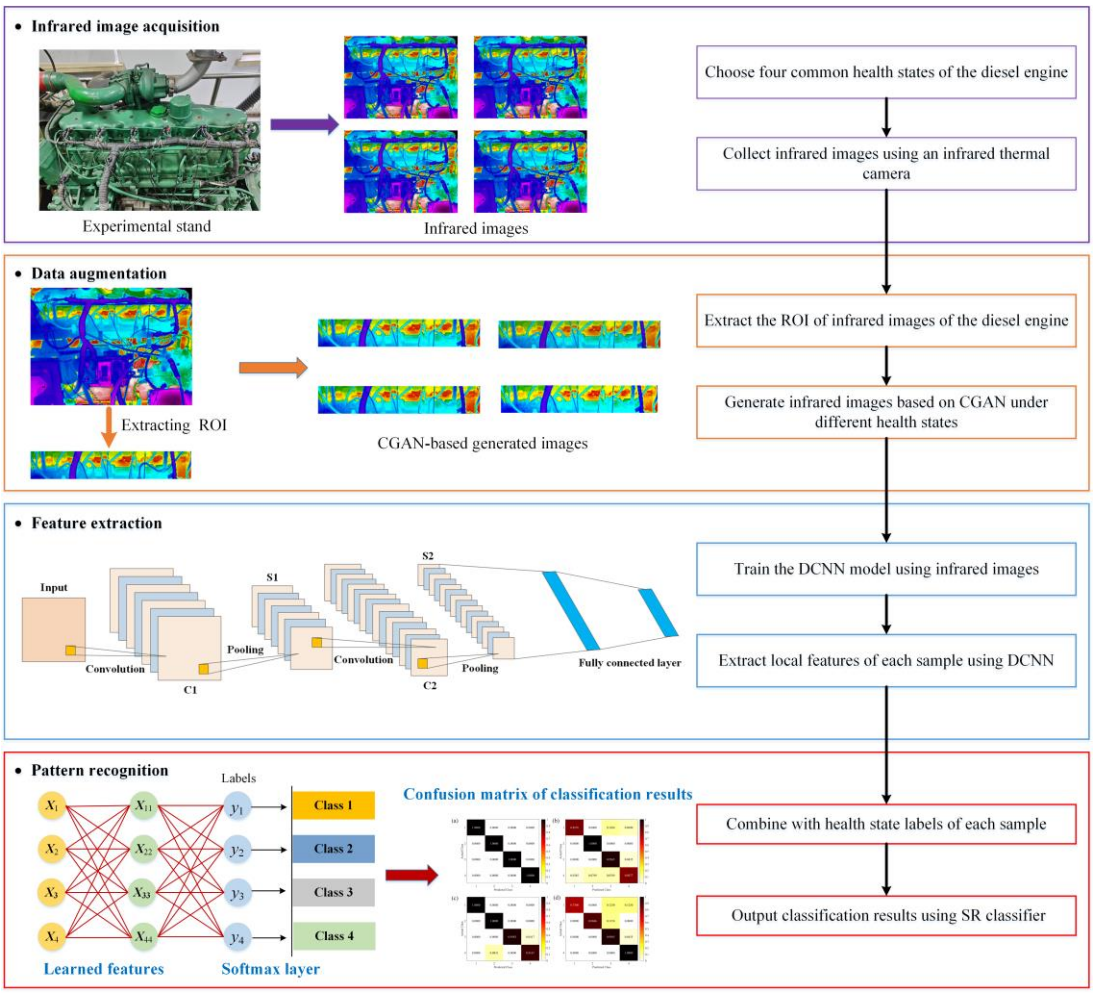

Fig. 10. Procedure of the proposed method.

5.1. Experiment description and infrared image acquisition

As a typical reciprocating mechanical equipment, diesel engines have a harsh operating environment and complex work tasks, making it more difficult to carry out effective fault diagnosis. Compared with the traditional fuel injection system, high-pressure common rail technology has precise fuel injection control, better fuel economy, lower emissions, lower noise and vibration, and higher power performance, and is now widely used in various types of machinery and equipment engines. In this paper, we take the high-pressure common rail diesel engine test bench as an example to carry out the research of diesel engine fault diagnosis methods using IRT. In the infrared image analysis, the cylinder head temperature change of the diesel engine directly reflects the working status of the fuel injection system, and intake and exhaust system, therefore, it is very relevant and engineering practical significance to collect the infrared image signals under different health states for fault diagnosis research in the cylinder head area of the diesel engine.

The paper relies on the condition monitoring experimental bench of the CA6DF3-20E3 high-pressure common rail diesel engine in the university laboratory for infrared image acquisition, which mainly includes two parts: the diesel engine and control panel, in addition, a MAG32 infrared thermal camera and a data acquisition system are deployed for infrared image acquisition. The basic composition and actual arrangement of the above equipment are shown in Figure 11.

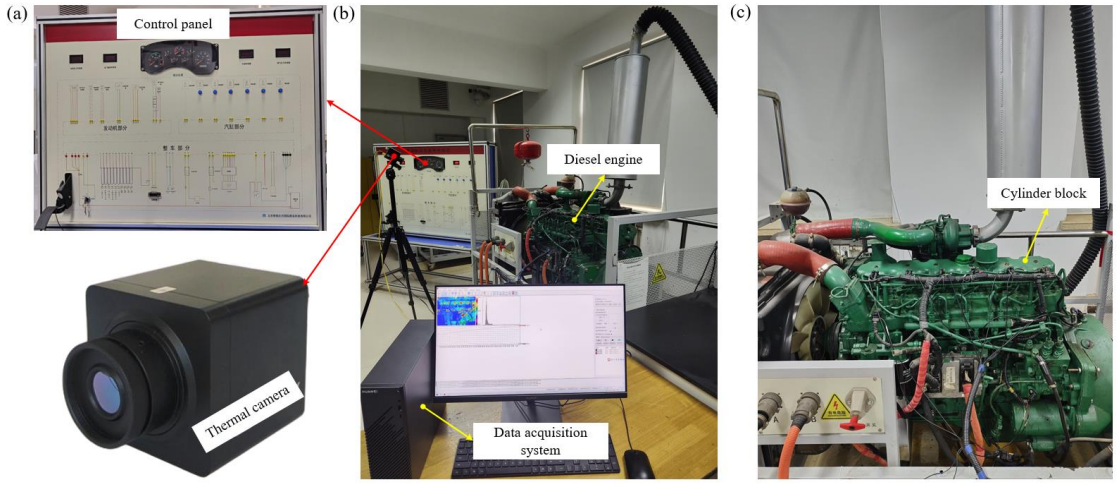

Fig. 11. (a) Enlarged views of the infrared thermal camera and control panel; (b) IRT-based diesel engine condition monitoring system; (c) Diesel engine.

As shown in Figure 11, the start and shutdown of the diesel engine is mainly controlled by the switch on the control panel, and the real-time status information such as speed, intake pressure, oil quantity and water temperature can also be read from the control panel, and the speed and output of the diesel engine are adjusted using the accelerator pedal. The technical parameters of the diesel engine and the infrared thermal camera used in the experiment are shown in Table 1.

Table 1. Technical parameters of the diesel engine and infrared thermal camera.

Diesel engine		Infrared thermal camera	
Common rail mode	BOSCH electronic control	Infrared detector type	Uncooled focal plane
Air intake mode	Supercharged intercooling	Image resolution	384×288
Rated power	155 KW	Frame rate	50fps
Rated speed	2300 r/min	Measuring range	-20℃~150℃
Maximal torque	760NM	Ambient temperature	19.2℃
Compression ratio	17.4	Measuring sensitivity	0.02℃
Total displacement	6.7 L	Emissivity	0.94
Number of cylinders	6	Test distance	1.2m

During the experiment, four types of faults, including normal condition (NC), single-cylinder misfire (SCM), multi-cylinder misfire (MCM), and air filter blockage (AFB), were introduced into the diesel engine. Note that SCM and MCM are simulated by disconnecting the cylinder ignition power line, and an outer cover is added to the air filter to simulate AFB. The above fault patterns of the diesel engine are shown in Figure 12.

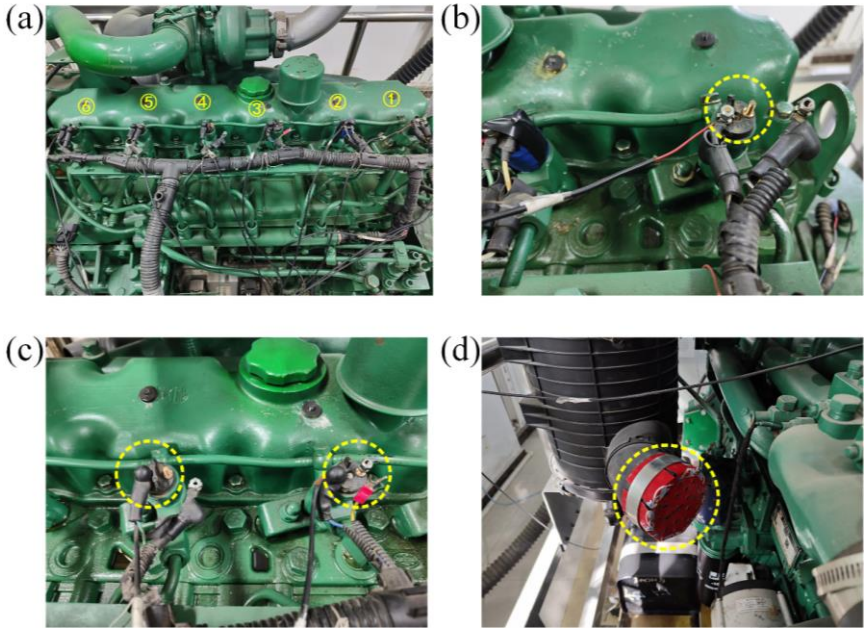

Fig. 12. (a) NC；(b) SCM；(c) MCM；(d) AFB.

In Figure 12(a), the six cylinders of the engine are labeled as ①-⑥, and the specific manifestations of SCM and MCM are misfire of cylinder 1, cylinder 3 and cylinder 4 at the same time, respectively. The engine speed was fixed at 500 rpm and the infrared images of the diesel engine were acquired using an infrared thermal camera following the steps detailed in Algorithm 1.

Algorithm 1. Steps for the infrared image acquisition of the diesel engine

Step 1. Select one of the four simulated fault types.

Step 2. Before starting the experiment, the infrared thermal camera parameters were set, and at this time the diesel engine and room ambient temperatures were consistent, both at 19.2°C.

Step 3. The diesel engine speed was set to a constant 500 rpm and one infrared image was acquired every 10s.

Step 4. The experiment time was set to 25 minutes, and the maximal surface temperature of the cylinder had stabilized to 51.5°C by the end of the experiment. 150 infrared images were finally acquired for each fault type.

Step 5. Cool the diesel engine to room temperature sufficiently, keep the parameters such as image acquisition equipment, distance, angle, ambient temperature and humidity unchanged, and repeat Step 1 through Step 4 for the other three fault types until data collection is complete.

Note: In the experiment, air conditioners and humidifiers are used to adjust the indoor temperature and humidity.

It should be noted that the reason why an infrared image is collected every 10s is because the maximal acquisition frequency of the infrared thermal camera used in the experiment is every 3s to collect an infrared image. Subject to the hardware limitations, the infrared thermal camera manufacturer suggested that the best acquisition frequency should be set to collect an infrared image every 10s, to ensure that as much experimental data as possible can be collected in a limited period of time, and at the same time, the imaging quality of the infrared thermal camera can be guaranteed. On the other hand, an important topic of this paper is the early fault diagnosis of diesel engines. In the actual operation process, the faults of diesel engines may occur at any moment during the operation process. Therefore, at the early stage of diesel engine operation, the lack of training data due to the short start-up time exists objectively, and the significance of early fault diagnosis research lies in detecting whether the diesel engine has a fault state in the shortest possible time.

5.2 Process of infrared image data augmentation

Before performing infrared image data augmentation, the ROI of infrared images are first extracted to narrow down the processing of image data to focus on the cylinder area with obvious temperature changes to reduce the interference of redundant information in the images. Extracting image ROI is a common task in the field of image processing and CV, which can effectively reduce the computational effort of image processing, better image feature extraction, and improve the efficiency and speed of image processing. In the field of CV, extracting ROI has a wide range of applications in tasks such as image classification, target detection, and target tracking [52]. The infrared image of the diesel engine under NC after 20 minutes of stable operation is selected and shown in Figure 13.

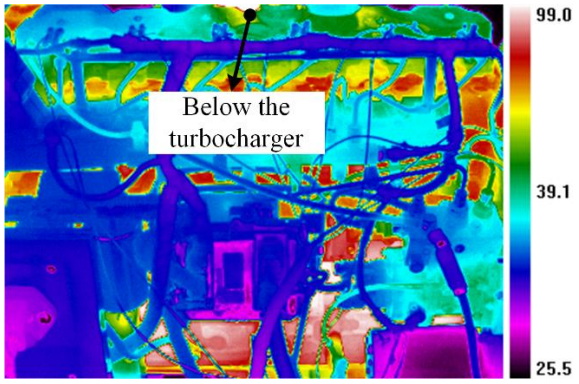

Fig. 13. The infrared image of the diesel engine under NC after 20 minutes of steady operation.

In Figure 13, the temperature unit is °C. The observation shows that the infrared image expresses the temperature distribution on the surface of the diesel engine in a visualized form, however, it also contains many disturbing factors that affect the analysis. For example, in the whole infrared image, the areas with higher temperature and obvious brightness are mainly the cylinder block area, the top turbocharger area, the bottom battery area and individual scattered locations where the brightness and temperature are the highest below the turbocharger.

Further analysis shows that diesel engine infrared images have the following unique characteristics compared to other types of infrared images or visible light pictures:

(1) Temperature distribution characteristics: infrared images of the diesel engine reflect the temperature distribution inside the engine. By observing the infrared images, the hot and cold spots inside the engine can be clearly seen. These hot and cold spots reflect the heat flow and heat dissipation inside the engine.

(2) Visualization of the combustion process: infrared images can visualize the process of diesel combustion in the combustion chamber. When diesel fuel burns, it releases a large amount of heat, which can be visualized by infrared images. By observing the infrared image, we can clearly perceive the shape and size of the combustion chamber, as well as the distribution of diesel fuel in the combustion chamber.

(3) Fault diagnosis: infrared images can be used for fault detection and diagnosis. For example, by observing infrared images, problems such as engine misfire, oil leakage, gas leakage and blockage can be found. At the same time, the performance changes and aging of the engine can be assessed by comparing the differences in the infrared images at different points in time.

(4) Condition monitoring: infrared images can be used for real-time monitoring of the engine operating condition. For example, the workload, operating efficiency and emissions of the the engine can be understood through observing the infrared images, which is important for evaluating the performance of the engine and maintaining the normal operation.

Moreover, different faults also have corresponding characteristics in infrared images of the diesel engine. For example, (1) The cylinder temperature will have a certain temperature increase under normal operation conditions, but when a misfire occurs in a certain cylinder of the engine, the cylinder temperature will obviously rise beyond the normal working range due to incomplete combustion or inaccurate ignition timing, which makes the infrared image locally bright. (2) The temperature rise caused by AFB may be uneven. In an infrared image, it can be observed that the regional temperature distribution is uneven, and the size or shape of hot spots are inconsistent. Large and obvious hot spots may be formed in areas with serious blockage. (3) The starting failure in the diesel engine may be caused by the serious wear of the inner wall of the cylinder, the excessive gap between the cylinder liner and the piston ring, the air leakage of the valve, and the failure of the fuel injection pump or the blockage of the fuel injection nozzle. Then, abnormal temperature distribution or uneven hot spots may be displayed in infrared images.

In conclusion, infrared images of the diesel engine offer

unique advantages in terms of temperature distribution characteristics, combustion process visualization, fault diagnosis, and operation status monitoring. These advantages make IRT a powerful non-destructive testing and diagnostic tool with a wide range of applications in the field of fault diagnosis of diesel engines.

Furthermore, some of the extraneous elements such as wiring, piping and other parts of the test bench can also cause greater interference to the infrared image analysis. Therefore, before data augmentation of the infrared image, the image ROI needs to be extracted, the significance of which is to reduce the influence of interfering factors and facilitate the next step of feature extraction. The resolution of the infrared image acquired in this study is 384×288, and after extracting the ROI for the diesel engine block part, the resolution is 360×50, as shown in Figure 14.

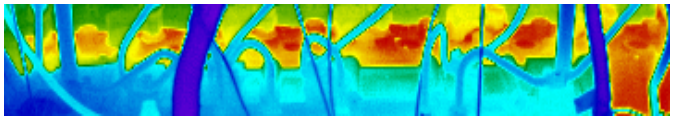

Fig. 14. The Infrared image ROI of the diesel engine under NC

After the ROI extraction operation, the infrared image size is reduced from 324 kb to 52.7 kb, indicating that the ROI extraction can effectively reduce the amount of data to be processed, thus improving the speed and efficiency of subsequent fault pattern identification. In the next step, the extracted ROI is input to the CGAN model for data augmentation, as shown in Figure 15.

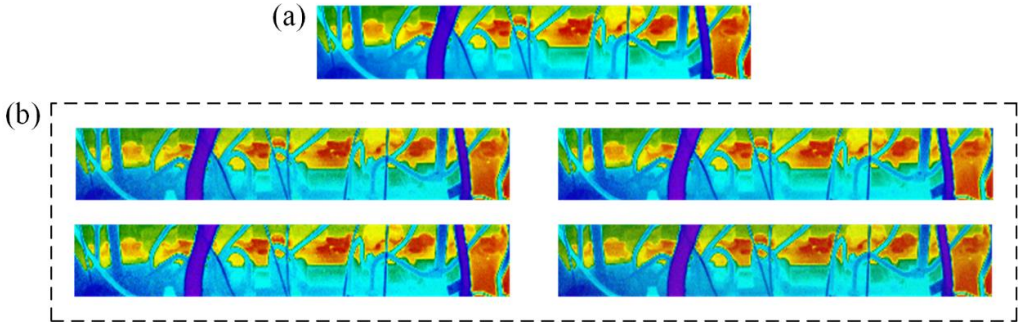

Fig. 15. (a) The original infrared image ROI under NC; (b) Examples of the infrared image ROI under NC generated by CGAN.

Analysis of Figure 15 shows that CGAN learns how to generate images from random noise corresponding to the given conditions by means of adversarial training, so that the generated images have the same distribution as the original images, achieving a good image generation effect and thus data augmentation.

6. Experiment validations

6.1. Experimental dataset description

The diesel engine operation process is usually accompanied by significant temperature changes. In this experiment, the average temperature of the cylinder surface continued to rise from 19.2℃ at the initial operation to 51.5℃ and then remained basically stable. In this case, an infrared image was acquired every 10s using the infrared thermal camera for 25 minutes, and finally 150 infrared images were acquired for each fault type. In this study, four effective DL models such as DCNN, stacked auto-encoder (SAE), recurrent neural network (RNN), and deep neural network (DNN) will be applied for infrared image feature extraction and combined with SR classifier for fault pattern recognition.

To investigate the early fault diagnosis performance of each model, this paper uses two datasets for the validation of related models, including dataset 1 and dataset 2. Specifically, based on the ROI extraction of infrared images, the acquisition time of each fault type is divided into 5 parts equally, and there are 30 samples in each time zone, then dataset 1 is a sample grid consisting of 5 time zones, including zone 1 (0-5min), zone 2 (5-10min), zone 3 (10-15min), zone 4 (15-20min), and zone 5 (20-25min), each zone is 5 minutes long and contains 120 samples (4 fault types × 30 samples). Dataset 2, on the other hand, is based on the original data and is augmented with data using CGAN. The specific operation is as follows: the infrared images in a single time zone under each fault type are used as the original images, and constraints such as image size and number are added to generate 90 infrared images, i.e., the sample size in a single time zone under each fault type is expanded from 30 to 120, and the total sample size of dataset 2 eventually reaches 4 times that of dataset 1. For example, the

infrared images under four fault types in zone 3 of Dataset 1 are shown in Figure 16.

It is uniformly stated that the concepts such as early fault diagnosis and early operation stage of the diesel engine mentioned in the following of this paper are for time zone 1, i.e., the first 5 minutes of diesel engine operation.

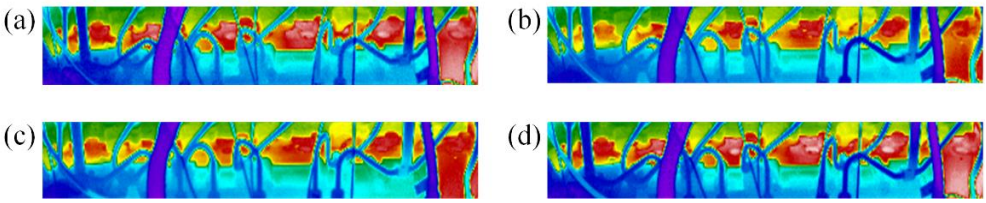

Fig. 16. Infrared images of diesel engines of four fault types: (a) NC, (b) SCM, (c) MCM, (d) AFB.

As shown in Figure 16, the differences between the infrared images of different fault types are very small under the effect of heat conduction of mechanical equipment, and it is difficult to distinguish them visually, so artificial intelligence (AI) techniques need to be introduced to assist in decision making. In this paper, the training and test sets are randomly divided according to the ratio of 8 to 2 for evaluating the performance of the model and adjusting the hyperparameters of the model. Specific descriptions of individual temporal zones in dataset 1 and dataset 2 are given in Table 2 and Table 3, respectively.

Table 2. Detailed description of a single zone in dataset 1.

Fault types	Class labels	Number of training images	Number of test images
NC	1	24	6
SCM	2	24	6
MCM	3	24	6
AFB	4	24	6

Table 3. Detailed description of a single zone in dataset 2

Fault types	Class labels	Number of training images	Number of test images
NC	1	96	24
SCM	2	96	24
MCM	3	96	24
AFB	4	96	24

It is worth noting that in the paper, due to the limitation of time and experimental equipment, experimental data was collected for each fault mode only once. However, to ensure that this single experiment's results are not influenced by other factors leading to potential errors, it may be more meaningful to conduct multiple sets of experiments for each fault mode, and this aspect will be specifically developed in the future research.

6.2. Parameter setting of the involved DL models

In the paper, four DL models such as DCNN, SAE, RNN, and DNN are used for infrared image feature extraction, and finally, SR classifier is deployed for fault pattern recognition. Therefore, for DCNN, this paper uses the AlexNet model for feature parameter extraction. AlexNet model has a complex network structure consisting of multiple convolutional layers (CL), pooling layers (PL) and fully connected layers (FCL), and also uses ReLU activation function, dropout regularization and other techniques, which has the advantages of high accuracy and scalability. The emergence of AlexNet marks the rise of DCNN, which has led to significant progress in research in the field of CV. The detailed structure of the AlexNet model is shown in Table 4.

Table 4. Model structure and parameter settings of AlexNet.

Layers	Number of convolution kernels	Convolution kernel size	Input size	Output size	stride	padding
Input layer	/	/	227×227×3	/	/	/
CL 1	96	11×11	227×227×3	55×55×96	4×4	0
PL 1	1	3×3	55×55×96	27×27×96	2×2	/
CL 2	256	5×5	27×27×96	27×27×256	1×1	2×2
PL 2	1	3×3	27×27×256	13×13×256	2×2	/
CL 3	384	3×3	13×13×256	13×13×384	1×1	1×1
CL 4	384	3×3	13×13×384	13×13×384	1×1	1×1
CL 5	256	3×3	13×13×384	13×13×256	1×1	1×1
PL 3	1	3×3	13×13×256	6×6×256	2×2	/
FCL 1	/	/	6×6×256	4096	/	/
FCL 2	/	/	4096	2048	/	/
FCL 3	/	/	2048	4	/	/
Output layer	/	/	/	4	/	/

To verify the effectiveness and superiority of DCNN, DL models such as SAE, RNN and DNN are applied for comparative analysis. In the study of the paper, the long short-term memory (LSTM) neural network and multilayer perceptron (MLP) in RNN and DNN are deployed for fault feature extraction and pattern recognition, respectively. The detailed parameter settings of the above models are shown in Table 5.

Table 5. Parameter settings for releted comparison models.

Models	Size of the networks	Activation functions	Classifiers
SAE	[54000, 1024, 512, 128, 4]	ReLU	Softmax
LSTM	[54000, 100, 100, 4]	Sigmoid	Softmax
MLP	[54000, 512, 256, 128, 4]	ReLU	Softmax

6.3. Results and discussion

In the practical application of diesel engines, functional faults may occur at various stages of the operation process. Therefore, to prevent possible early faults and perform timely fault diagnosis and troubleshooting, this case divides the working process of the diesel engine according to time, aiming to verify the effectiveness of the data augmentation method proposed in this paper for early fault diagnosis of diesel engines. At the same time, the fault diagnosis results are compared with the DL models such as SAE, LSTM, and MLP to prove the superiority of the DCNN-based fault diagnosis method proposed in the paper.

First, based on dataset 1, the above four DL models were used for fault pattern recognition, and each model was trained and tested 10 times for different time zones, and the specific classification results are shown in Table 6 and Figure 17, respectively.

Table 6. Classification results of dataset 1.

Models		Time zones					Average
		0-5min	5-10 min	10-15 min	15-20 min	20-25 min	
DCNN	Accuracy	65.42%	97.91%	99.58%	99.17%	100%	92.42%
	Std	0.0647	0.0208	0.0125	0.0250	0	0.0246
SAE	Accuracy	59.35%	93.33%	95%	90.42%	89.58%	85.54%
	Std	0.0648	0.0333	0.0947	0.0895	0.1074	0.0780
LSTM	Accuracy	57.08%	97.50%	95.83%	97.50%	100%	89.58%
	Std	0.0933	0.0276	0.0559	0.0382	0	0.0430
MLP	Accuracy	62.50%	95.83%	96.25%	97.50%	97.08%	89.83%
	Std	0.0833	0.0417	0.0542	0.0425	0.0647	0.0573

Note: Std represents standard deviation.

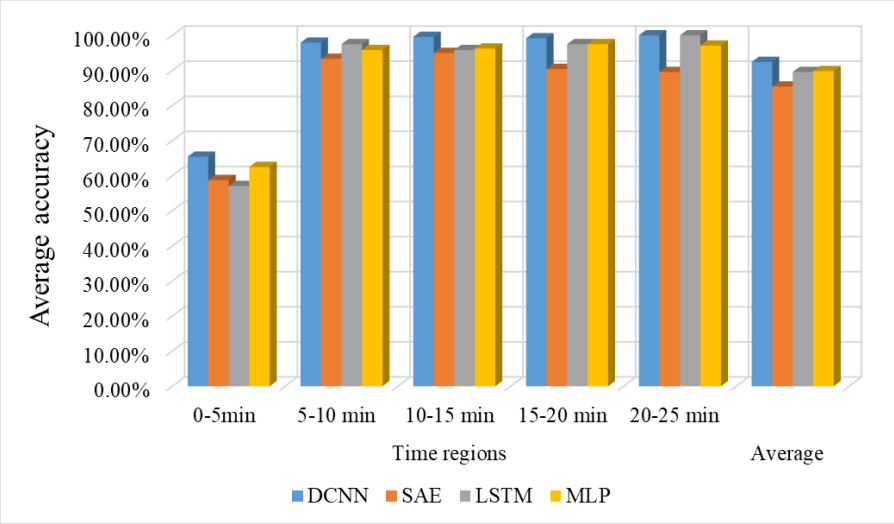

Fig. 17. Diagnostic accuracy of DCNN, SAE, LSTM and MLP in five time zones of dataset 1.

As seen in Table 6 and Figure 17, the average diagnostic accuracy of DCNN is the highest in all five independent time zones of dataset 1, and the overall average diagnostic accuracy is also the highest among the four models, reaching 92.42%. The other three models performed differently within each time zone, among which, MLP ends up with the second highest average diagnostic accuracy after DCNN with 89.83%, while SAE and LSTM have lower average diagnostic accuracies of 85.54% and 89.58%, respectively.

In terms of early fault diagnosis performance, the

classification accuracy of the four DL models for different fault patterns in the early operation stage of the diesel engine is mainly analyzed. First, it can be seen that the early fault diagnosis accuracy of all four DL models is low. Obviously, the early fault diagnosis accuracy of DCNN is 65.42%, which is still the highest among the four models, and LSTM has the lowest accuracy, which is only 57.08%. In terms of algorithm stability, the proposed DCNN method also has better performance, with the lowest standard deviation of 0.0246 among the four models in terms of diagnostic accuracy within a single time zone and during the whole operation process, while SAE has the highest standard deviation of 0.0780.

To show the performance of DCNN, SAE, LSTM, MLP in early fault diagnosis of the diesel engine, the confusion matrix of classification results of the above four models for the data of zone 1 in dataset 1 is shown in Figure 18.

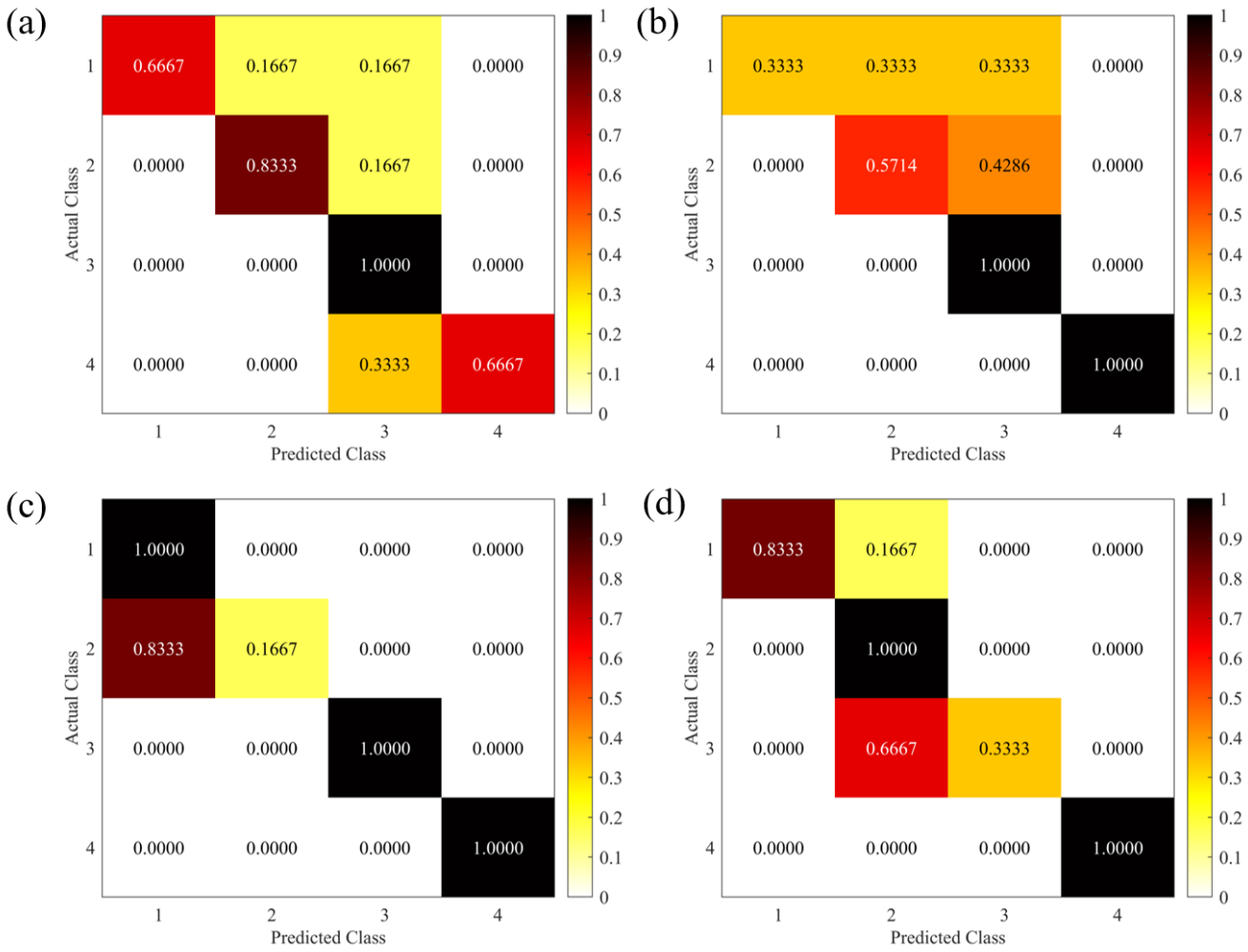

Fig. 18. Classification results of four methods for zone1 of dataset 1: (a) DCNN; (b) SAE; (c) LSTM; (d) MLP.

In Figure 18, the highest diagnostic accuracy among the 10 training and testing results is taken for each DL model. As can be seen from Figure 18, at the early operation stage of the diesel engine, the cylinder temperature and room temperature are close to each other, and the amount of model training data is insufficient, which causes some interference to the early fault diagnosis. By analyzing the above experimental results, it can be concluded that under the condition of dataset 1, the diagnostic accuracy of all four DL models for zone 1 is below 80%, but from zone 2 onwards, the accuracy of each model has improved significantly, which indicates that the existing methods are not well adapted to early fault diagnosis task of the diesel engine. Therefore, it is important to study how to improve the early fault diagnosis accuracy of the diesel engine as much as possible based on the limited training data. In this paper, we propose a CGAN-based data augmentation method to expand the amount of data in the early operation stage of the diesel engine and apply DL models such as DCNN for fault pattern recognition. With the early fault diagnosis technology, we can detect diesel engine faults in time, reduce engine downtime due

to faults, improve equipment reliability, reduce maintenance costs and machine downtime, and thus reduce production costs and improve economic efficiency.

Based on dataset 2, DCNN, SAE, LSTM, MLP are used for fault pattern recognition, and each model is trained and tested 10 times for different time zones, and the specific classification results are shown in Table 7 and Figure 19, respectively.

Table 7. Classification results of dataset 2.

Models		Time zones					Average
		0-5min	5-10 min	10-15 min	15-20 min	20-25 min	
DCNN	Accuracy	98.23%	100%	100%	100%	100%	99.65%
	Std	0.0148	0	0	0	0	0.0030
SAE	Accuracy	81.67%	100%	100%	100%	100%	96.33%
	Std	0.0502	0	0	0	0	0.0100
LSTM	Accuracy	94.27%	100%	100%	100%	100%	98.85%
	Std	0.0149	0	0	0	0	0.0030
MLP	Accuracy	81.58%	99.38%	100%	99.69%	100%	96.13%
	Std	0.0633	0.0125	0	0.0094	0	0.0170

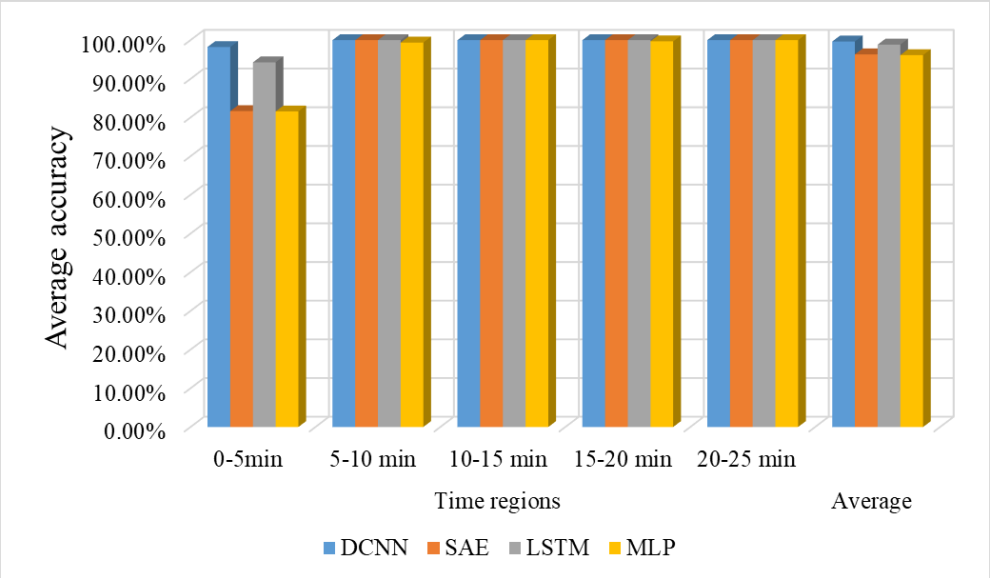

Fig. 19. Diagnostic accuracy of DCNN, SAE, LSTM and MLP in five time zones of dataset 2.

As can be seen from Table 7 and Figure 19, the average diagnostic accuracy of DCNN is the highest or tied for the highest in all five independent time zones of dataset 2, and the overall average diagnostic accuracy is also the highest among the four models, reaching 99.65%. In addition, LSTM ends up with the second highest average diagnostic accuracy after DCNN, reaching 98.85%, while SAE and MLP have relatively lower average diagnostic accuracies of 96.33% and 96.13%, respectively.

In terms of early fault diagnosis performance, in line with the previous study, we mainly analyze the classification accuracy of the four DL models for different fault patterns in the early operation stage of the diesel engine. First, it can be clearly seen that the early fault diagnosis accuracy of all four DL models has improved significantly after CGAN-based data augmentation of the dataset. Among them, the early fault diagnosis accuracy of DCNN is 98.23%, which is still the highest among the four models, and the lowest accuracy is MLP, which is 81.58%. Secondly, the algorithm stability of the four DL models has also achieved a substantial improvement. The DCNN proposed in this paper also has the best performance in terms of algorithm stability, and its standard deviation of diagnostic accuracy is the lowest among the four models in a single time zone and the whole operation process, which is 0.0030. Meanwhile, the standard deviation of diagnostic accuracy of MLP is the largest, reaching 0.0170.

Furthermore, in order to show the performance of DL models in early fault diagnosis of the diesel engine after applying the CGAN-based data augmentation method, the confusion matrix of the classification results of the above four models for the data of zone 1 in dataset 2 is shown in Figure 20.

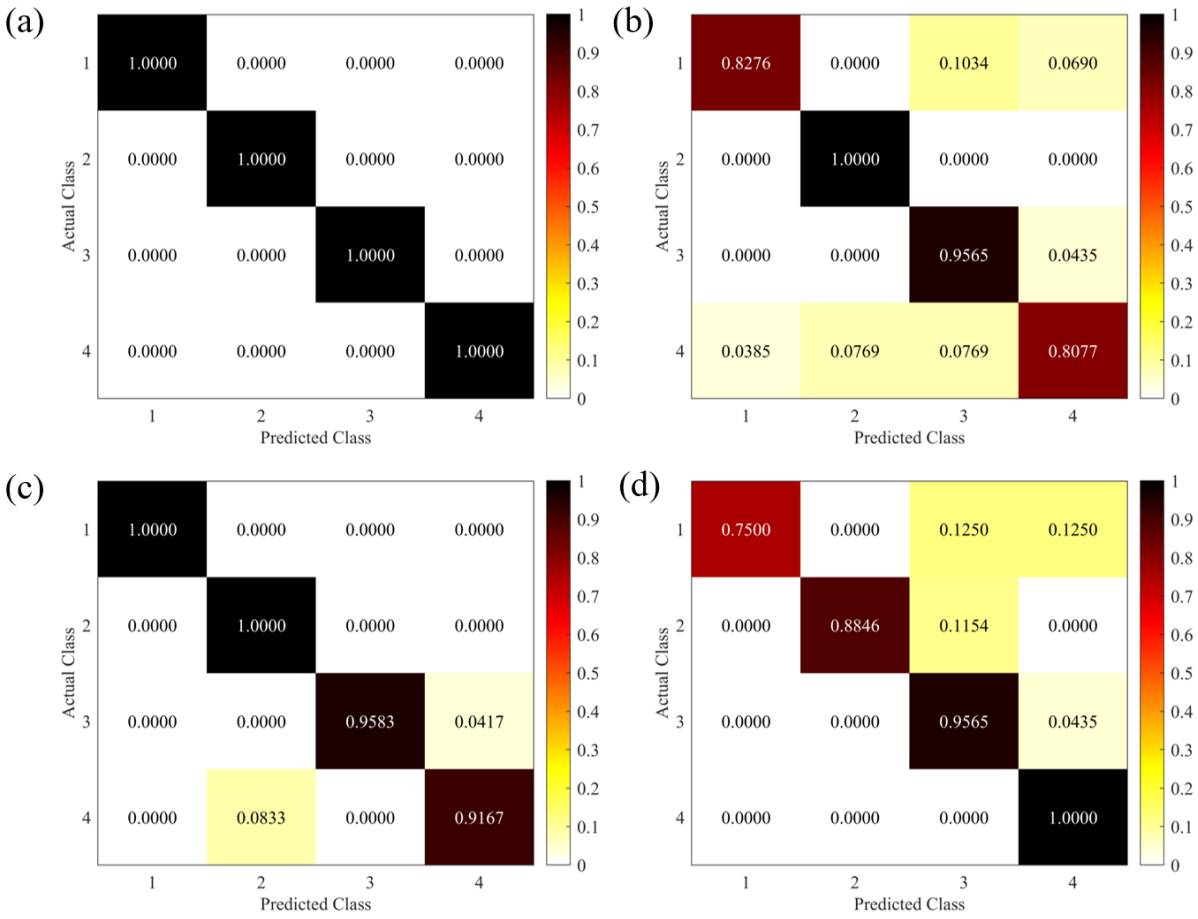

Fig. 20. Classification results of four models for the data of zone 1 in dataset 2: (a) DCNN; (b) SAE; (c) LSTM; (d) MLP.

In Figure 20, the highest diagnostic accuracy among the 10 training and testing results is taken for each DL model. Since all the above four DL models used the SR classifier for fault pattern recognition, the analysis results for dataset 1 and dataset 2 can show that DCNN has better infrared image feature extraction capability, which is more beneficial for subsequent fault pattern recognition. Moreover, during the 25 minutes of diesel engine operation, a large part of the time is in the state of gradual temperature rise, so the classification results of both dataset 1 and dataset 2 can achieve the highest fault diagnosis accuracy and the lowest standard deviation, which proves that DCNN has better algorithm stability and stronger resistance to temperature fluctuation interference when performing fault pattern recognition of the diesel engine.

To quantify the effect of CGAN-based data augmentation method on the improvement of fault diagnosis accuracy of DCNN, SAE, LSTM, MLP in the early operation stage and whole operation cycle of the diesel engine, the related calculation results are shown in Table 8 and Table 9.

Table 8. Comparison results of the average fault diagnosis accuracy and its standard deviation for dataset 1 and dataset 2 over the whole operation cycle

Models	Dataset	Accuracy	Comparison 1	Std	Comparison 2
DCNN	Dataset 1	92.42%	7.82%	0.0246	87.80%
	Dataset 2	99.65%		0.0030	
SAE	Dataset 1	85.54%	12.61%	0.0780	87.18%
	Dataset 2	96.33%		0.0100	
LSTM	Dataset 1	89.58%	10.35%	0.0430	93.02%
	Dataset 2	98.85%		0.0030	
MLP	Dataset 1	89.83%	7.01%	0.0573	70.33%
	Dataset 2	96.13%		0.0170	

Table 9. Comparison results of the average fault diagnosis accuracy and its standard deviation for data of zone 1 under dataset 1 and dataset 2

Models	Dataset	Accuracy	Comparison 1	Std	Comparison 2
DCNN	Dataset 1	65.42%	50.15%	0.0647	77.13%
	Dataset 2	98.23%		0.0148	
SAE	Dataset 1	59.35%	37.61%	0.0648	22.53%
	Dataset 2	81.67%		0.0502	
LSTM	Dataset 1	57.08%	65.15%	0.0933	84.03%
	Dataset 2	94.27%		0.0149	
MLP	Dataset 1	62.50%	30.53%	0.0833	24.01%
	Dataset 2	81.58%		0.0633	

In Table 9, Comparison 1 and Comparison 2 indicate the degree of improvement in fault diagnosis accuracy and the

degree of decrease in its standard deviation before and after data augmentation using CGAN, respectively. According to Table 6 and Table 7, the comparative results of fault diagnosis accuracy of DCNN, SAE, LSTM, and MLP in five time zones during the diesel engine operation are shown in Figure 21.

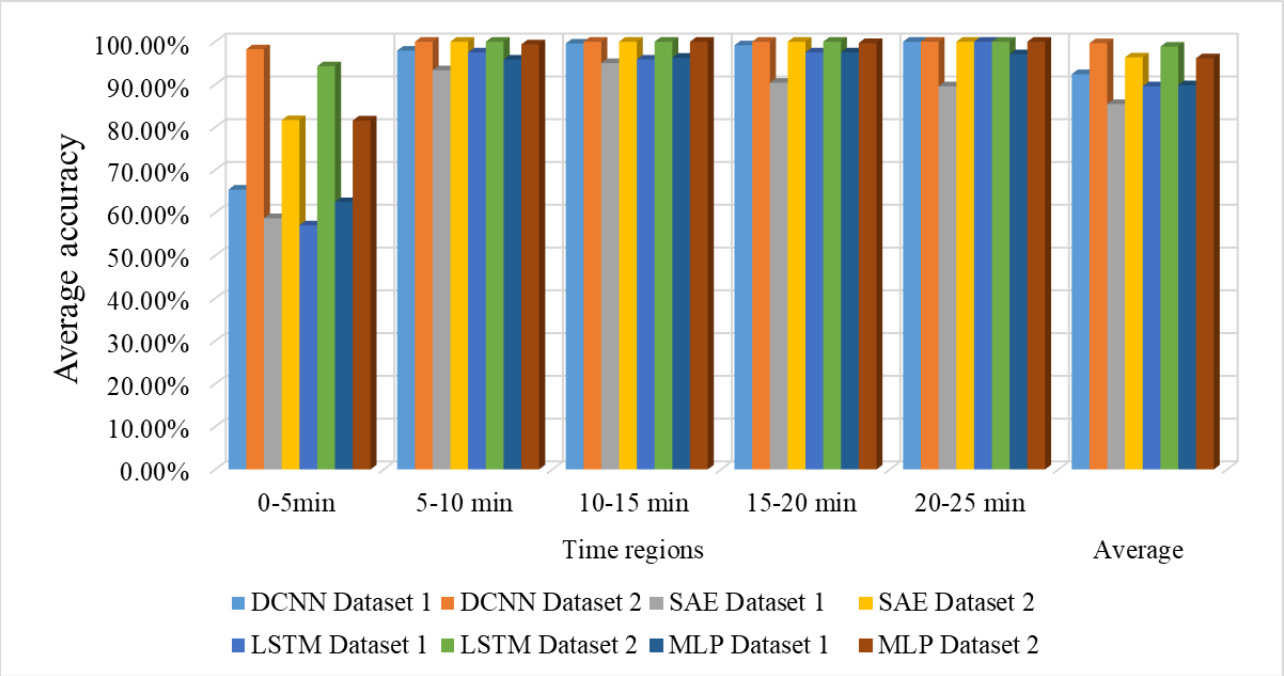

Fig. 21. Comparison results of diagnostic accuracy of DCNN, SAE, LSTM and MLP in five time zones.

According to Table 8, Table 9, and Figure 21, it is evident that after data augmentation based on CGAN, the average diagnostic accuracy of the above four models has been improved to a certain extent in various time zones and overall. SAE has the highest overall average accuracy improvement, reaching 12.61%, while LSTM has the highest early fault diagnosis accuracy improvement, reaching 65.15%. In terms of algorithm stability, the above four models have significantly improved in various time zones and overall. LSTM has the most significant reduction in overall and early fault diagnosis accuracy standard deviation, reaching 93.02% and 84.03%, respectively.

Furthermore, as can be seen from Table 2 and Table 3, zone 1 after data augmentation has 480 infrared images, while the whole time zone before data augmentation contains 600 infrared images. By comparing the accuracy of dataset 1 in Table 8 and dataset 2 in Table 9, it can be concluded that the accuracy of the diesel engine early fault diagnosis has been greatly improved after data augmentation, in which the accuracy of early fault diagnosis of DCNN and LSTM has exceeded the accuracy in the whole time zone, while the accuracy of SAE and MLP has reached the comparable level as that in the whole time zone. It is enough to prove that a small number of datasets can yield comparable classification accurately when expanded through data augmentation methods as compared to a large real-world dataset.

In summary, it can be concluded that the data augmentation method based on CGAN proposed in the paper can greatly improve the accuracy and algorithm stability of DL models for fault diagnosis of the diesel engine. Moreover, relevant experimental results indicate that DCNN has better feature extraction ability and algorithm stability compared to SAE, LSTM, and MLP, especially solving the engineering problem of low early fault diagnosis of diesel engines. The accuracy of early fault diagnosis based on DCNN can reach 98.23%. Therefore, the proposed IRT-DCNN based fault diagnosis method for diesel engines using CGAN based data augmentation has strong theoretical and practical value.

6.4. Effect evaluation of data augmentation

Before extracting infrared image features, this paper uses a data augmentation method based on CGAN to generate infrared images under certain constraints, to achieve the effect of data expansion. From Figure 14, it can be seen that the infrared image generated by CGAN is very close to the original image.

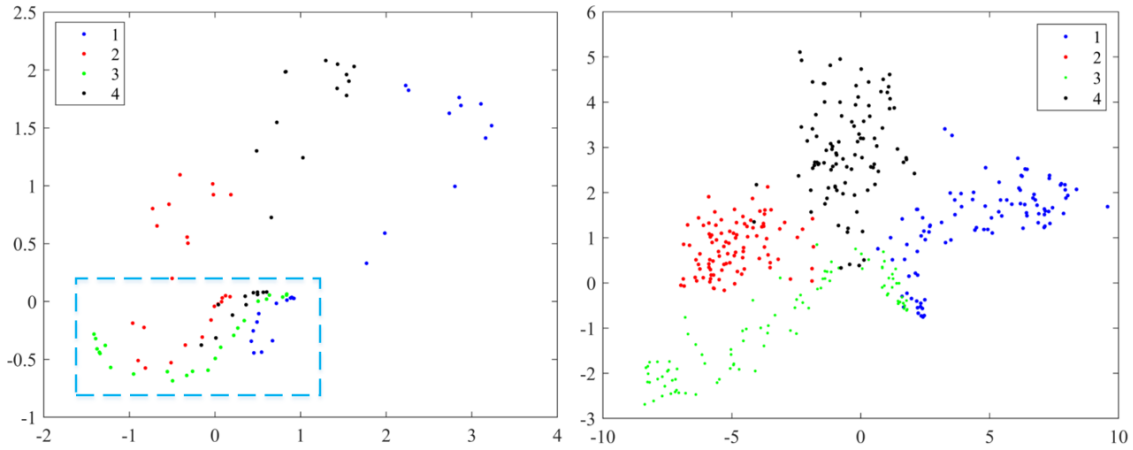

(a) Before CGAN (b) After CGAN

Fig. 22. Comparison of feature visualization before and after CGAN-based data augmentation.

To verify the role of CGAN-based data augmentation method in early fault diagnosis of diesel engines, the features of DCNN after the last layer of the fully connected operation during fault pattern recognition are selected for visualization based on the data of zone 1 in dataset 1 and dataset 2, as shown in Figure 22.

It can be clearly seen from Figure 22 that after data augmentation based on CGAN, the separation of features has been greatly improved, which is conducive to further feature extraction and pattern recognition. To further verify the effect of data augmentation based on CGAN on fault pattern recognition of the diesel engine, dataset 3 and dataset 4 are constructed on the basis of original data, as shown in Table 10 and Table 11, respectively.

Table 10. Detailed description of dataset 3.

Fault types	Class labels	Number of training images	Number of test images
NC	1	120	30
SCM	2	120	30
MCM	3	120	30
AFB	4	120	30

Table 11. Detailed description of dataset 4.

Fault types	Class labels	Number of training images	Number of test images
NC	1	240	60
SCM	2	240	60
MCM	3	240	60
AFB	4	240	60

It should be noted that dataset 3 is the original data without zone division of the diesel engine operation process; dataset 4 is the result of data augmentation of dataset 3 using CGAN, and since dataset 3 itself is all the data of the diesel engine during 25 minutes of operation time, which is already more than sufficient, considering the limited computer resources, dataset 4 is only expanded to twice of dataset 3.

For dataset 3 and dataset 4, DCNN, SAE, LSTM, and MLP are trained and tested 10 times with the same settings of relevant network parameters, respectively, then the comparison results are shown in Table 12.

As can be seen from Table 12, the CGAN-based data augmentation method can effectively improve the accuracy of fault pattern recognition of the diesel engine.

Tab. 12. Comparison results of average fault diagnosis accuracy and its standard deviation for each model under dataset 3 and data set 4

Model	Dataset	Average accuracy	Comparison 1	Std	Comparison 2
DCNN	Dataset 3	95.83%	3.01%	0.0105	55.24%
	Dataset 4	98.71%		0.0047	
SAE	Dataset 3	91.91%	2.82%	0.0316	55.06%
	Dataset 4	94.50%		0.0142	
LSTM	Dataset 3	86.42%	9.97%	0.0439	60.59%
	Dataset 4	95.04%		0.0173	
MLP	Dataset 3	85.83%	8.40%	0.0648	36.73%
	Dataset 4	93.04%		0.0410	

Among the four DL models, DCNN has the highest average diagnostic accuracy of 98.71%, while MLP has a relatively low diagnostic accuracy of 93.04%, LSTM has the largest improvement in average diagnostic accuracy of 9.97%, and the other three DL models also have different degrees of improvement in fault diagnosis accuracy after CGAN based data augmentation. On the other hand, DCNN has the best algorithm stability and is least affected by the variation of cylinder surface temperature. After CGAN-based data augmentation, the algorithm stability of LSTM improved the most, whose standard deviation of the average fault diagnosis accuracy decreased by 60.59%, and the algorithm stability of the other three DL models also improved to different degrees.

7. Conclusions

In this paper, IRT is introduced into diesel engine condition monitoring, and a fault diagnosis method based on CGAN and DCNN of diesel engines is proposed. Aiming at the real problems such as low early fault diagnosis accuracy of diesel engines and high influence by temperature fluctuation, CGAN is used to perform data augmentation on infrared image datasets, and then DCNN is deployed to automatically extract infrared image fault features, and the effectiveness and superiority of the proposed method are verified by comparing and analyzing with DL models such as SAE, LSTM and MLP. In summary, the innovative work of this paper is as follows:

(1) An effective fault diagnosis method of diesel engines is proposed by combining IRT and DCNN, which can automatically extract fault features from infrared images, and the method has excellent algorithmic stability and resistance to temperature fluctuation interference;

(2) The CGAN-based data augmentation method applied in this paper can not only substantially improve the accuracy and algorithmic stability of early fault diagnosis of diesel engines, but also effectively improve the diagnosis accuracy and algorithmic stability throughout the operation process and in each time zone, and the method is also applicable to DL models such as SAE, LSTM and MLP;

(3) The experimental results show that the DCNN-based fault diagnosis method proposed in this paper has better classification effect and algorithm stability compared with SAE, LSTM and MLP, and can effectively identify different fault patterns.

References

1. Baranitharan P, Kumanan S, Sudhagar S. An intelligent novel approach for diesel engine life monitoring using infrared image processing technic. Environmental Progress and Sustainable Energy 2022; 41(1):e13712, https://doi.org/10.1002/ep.13712.
2. Bi X, Lin J, Tang D, et al. VMD-KFCM algorithm for the fault diagnosis of diesel engine vibration signals. Energies 2020; 13(1): 228, https://doi.org/10.3390/en13010228.
3. Chen Z, Duan J, Kang L, Qiu G. Supervised anomaly detection via conditional generative adversarial network and ensemble active learning. IEEE Transactions on Pattern Analysis and Machine Intelligence 2022; 45(6): 7781–7798, https://doi.org/10.1109/TPAMI.2022.3225476.
4. Choudhary A, Mian T, Fatima S. Convolutional neural network based bearing fault diagnosis of rotating machine using thermal images. Measurement 2021; 176: 109196, https://doi.org/10.1016/j.measurement.2021.109196.
5. Ciabattoni L, Ferracuti F, Freddi A, Monteri A. Statistical spectral analysis for fault diagnosis of rotating machines. IEEE Transactions on Industrial Electronics 2018; 65(5): 4301–4310, https://doi.org/10.1109/TIE.2017.2762623.
6. Courtrai L, Pham M T, Lefèvre S. Small object detection in remote sensing images based on super-resolution with auxiliary generative adversarial networks. Remote Sensing 2020; 12(19): 3152, https://doi.org/10.3390/rs12193152.
7. Dong J, Yin R, Sun X, et al. Inpainting of remote sensing SST images with deep convolutional generative adversarial network. IEEE Geoscience and Remote Sensing Letters 2019; 16(2): 173–177, https://doi.org/10.1109/LGRS.2018.2870880.
8. Engine D, Clearance V, Diagnosis F. Diesel engine valve clearance fault diagnosis based on improved variational mode decomposition and bispectrum. Energies 2019; 12(4): 661, https://doi.org/10.3390/en12040661.
9. Flett J, Bone G M. Fault detection and diagnosis of diesel engine valve trains. Mechanical Systems and Signal Processing 2016; (72–73): 316–327, https://doi.org/10.1016/j.ymssp.2015.10.024.
10. Gan C, Xiao J, Wang Z, et al. Facial expression recognition using densely connected convolutional neural network and hierarchical spatial attention. Image and Vision Computing 2022; 117: 104342, https://doi.org/10.1016/j.imavis.2021.104342.

11. Goodfellow I, Pouget-Abadie J, Mirza M, et al. Generative adversarial networks. Communications of the ACM 2020; 63(11): 139–144, https://doi.org/10.1145/3422622
12. Gu C, Qiao X, Li H, Jin Y. Misfire fault diagnosis method for diesel engine based on MEMD and dispersion entropy. Shock and Vibration 2021; https://doi.org/10.1155/2021/9213697.
13. He M, He D. Deep learning based approach for bearing fault diagnosis. IEEE Transactions on Industry Applications 2017; 53(3): 3057–3065, https://doi.org/10.1109/TIA.2017.2661250.
14. Hou L, Zou J, Du C, Zhang J. A fault diagnosis model of marine diesel engine cylinder based on modified genetic algorithm and multilayer perceptron. Soft Computing 2020; 24: 7603–7613, https://doi.org/10.1007/s00500-019-04388-3.
15. Isola P, Zhu J Y, Zhou T, Efros A A. Image-to-image translation with conditional adversarial networks. 2017 IEEE Conference on Computer Vision and Pattern Recognition (CVPR) 2017; pp. 5967-5976, https://doi.org/10.1109/CVPR.2017.632.
16. Janssens O, Schulz R, Slavkovikj V, Stockman K, Loccufier M, Walle R V D, Hoecke S V. Thermal image based fault diagnosis for rotating machinery. Infrared Physics and Technology 2015; 73: 78–87, https://doi.org/0.1016/j.infrared.2015.09.004.
17. Jia F, Lei Y, Lin J, et al. Deep neural networks: A promising tool for fault characteristic mining and intelligent diagnosis of rotating machinery with massive data. Mechanical Systems and Signal Processing 2016; 72–73: 303–315, https://doi.org/10.1016/j.ymssp.2015.10.025.
18. Jia Z, Liu Z, Vong C M, Pecht M. A rotating machinery fault diagnosis method based on feature learning of thermal images. IEEE Access 2019; 7: 12348–12359, https://doi.org/10.1109/ACCESS.2019.2893331.
19. Kowalski J, Krawczyk B, Woźniak M. Fault diagnosis of marine 4-stroke diesel engines using a one-vs-one extreme learning ensemble. Engineering Applications of Artificial Intelligence 2017; 57: 134–141, https://doi.org/10.1016/j.engappai.2016.10.015.
20. LeCun Y, Bottou L, Bengio Y, et al. Gradient-based learning applied to document recognition. Proceedings of the IEEE 1998; 86(11): 2278–2323, https://doi.org/10.1109/5.726791.
21. Lee W, Seong J J, Ozlu B, et al. Biosignal sensors and deep learning-based speech recognition: A review. Sensors 2021; 21(4): 1399, https://doi.org/10.3390/s21041399.
22. Lei Y, Jia F, Lin J, et al. An intelligent fault diagnosis method using unsupervised feature learning towards mechanical big data. IEEE Transactions on Industrial Electronics 2016; 63(5): 3137–3147, https://doi.org/10.1109/TIE.2016.2519325.
23. Li Y. Copy-move detection method based on conditional generative adversarial networks. Master's Thesis, University of Chinese Academy of Sciences 2021. (In Chinese)
24. Li Y, Du X, Wang X, Si S. Industrial gearbox fault diagnosis based on multi-scale convolutional neural networks and thermal imaging. ISA Transactions 2022; 129: 309–320, https://doi.org/10.1016/j.isatra.2022.02.048.
25. Li Y, Du X, Wan F, Wang X, Yu H. Rotating machinery fault diagnosis based on convolutional neural network and infrared thermal imaging. Chinese Journal of Aeronautics 2020; 33(2): 427–438, https://doi.org/10.1016/j.cja.2019.08.014.
26. Li Y, Gu J, Zhen D, Xu M, Ball A. An evaluation of gearbox condition monitoring using infrared thermal images applied with convolutional neural networks. Sensors 2019; 19(9): 2205, https://doi.org/10.3390/s19092205.
27. Liu H, Li L, Ma J. Rolling bearing fault diagnosis based on STFT-deep learning and sound signals. Shock and Vibration 2016; https://doi.org/10.1155/2016/6127479.
28. Liu Q, He X, Teng Q, Qing L, Chen H. BDNet: A BERT-based dual-path network for text-to-image cross-modal person re-identification. Pattern Recognition 2023; 141: 109636, https://doi.org/10.1016/j.patcog.2023.109636.
29. Liu Y, Lai K W C. The performance index of convolutional neural network-based classifiers in class imbalance problem. Pattern Recognition 2023; 137: 109284, https://doi.org/10.1016/j.patcog.2022.109284.
30. Mirza M, Osindero S. Conditional Generative Adversarial Nets. arXiv:1411.1784 2014; https://doi.org/10.48550/arXiv.1411.1784.
31. Molinier N, Painchaud-april G, Duff A L, Toews M, Bélanger P. Ultrasonic imaging using conditional generative adversarial networks. Ultrasonics 2023; 133: 107015, https://doi.org/10.1016/j.ultras.2023.107015.
32. Nikbakht R, Jonsson A, Lozano A. Unsupervised learning for parametric optimization. IEEE Communications Letters 2021; 25(3): 678–681, https://doi.org/10.1109/LCOMM.2020.3027981.
33. Pan M H, Xin H Y, Xia C Q, et al. Few-shot classification with task-adaptive semantic feature learning. Pattern Recognition 2023; 141:

109594, https://doi.org/10.1016/j.patcog.2023.109594.

34. Ramteke S M, Chelladurai H, Amarnath M. Diagnosis and classification of diesel engine components faults using time–frequency and machine learning approach. Journal of Vibration Engineering and Technologies 2022; 10: 175–192, https://doi.org/10.1007/s42417-021-00370-2.
35. Russakovsky O, Deng J, Su H, Krause J, Satheesh S, et al. ImageNet Large Scale Visual Recognition Challenge. International Journal of Computer Vision 2015; 115(3): 211–252, https://doi.org/10.1007/s11263-015-0816-y.
36. Shi G, Li Y, Qian Y. Research on the applications of infrared technique in the diagnosis and prediction of diesel engine exhaust fault. Journal of Thermal Science 2011; 20(2): 189–194, https://doi.org/10.1007/s11630-011-0456-7.
37. Su Q, Xi X, Yuan Y, et al. Application of ultrasonic infrared thermography technology in crack detection of aeroengine blades. Nondestructive Testing 2019; 41(4): 54-57. (In Chinese)
38. Sun J, Yan C, Wen J. Intelligent bearing fault diagnosis method combining compressed data acquisition and deep learning. IEEE Transactions on Instrumentation and Measurement 2018; 67(1): 185–195, https://doi.org/10.1109/TIM.2017.2759418.
39. Tran V T, Yang B S, Gu F, Ball A. Thermal image enhancement using bi-dimensional empirical mode decomposition in combination with relevance vector machine for rotating machinery fault diagnosis. Mechanical Systems and Signal Processing 2013; 38(2): 601–614, https://doi.org/10.1016/j.ymssp.2013.02.001.
40. Varshney D, Ekbal A, Tiwari M, Nagaraja G P. EmoKbGAN: Emotion controlled response generation using Generative Adversarial Network for knowledge grounded conversation. PLoS ONE 2023; 18(2): e0280458, https://doi.org/10.1371/journal.pone.0280458.
41. Verstraete D, Ferrada A, Droguett E L, et al. Deep learning enabled fault diagnosis using time-frequency image analysis of rolling element bearings. Shock and Vibration 2017; https://doi.org/10.1155/2017/5067651.
42. Wang R, Zhan X, Bai H, Dong E, Cheng Z, Jia X. A review of fault diagnosis methods for rotating machinery using infrared thermography. Micromachines 2022; 13(10): 1644, https://doi.org/10.3390/mi13101644.
43. Wang R, Chen H, Guan C. DPGCN model: A novel fault diagnosis method for marine diesel engines based on imbalanced datasets. IEEE Transactions on Instrumentation and Measurement 2023; 72: 1–11, https://doi.org/10.1109/TIM.2022.3228002.
44. Wang W, Li Q. Crack identification of infrared thermal imaging steel sheet based on convolutional neural network. MATEC Web of Conferences 2018; 232(11): 01053, https://doi.org/10.1051/matecconf/201823201053.
45. Wang Z, Xia H, Zhang J, Yang B, Yin W. Imbalanced sample fault diagnosis method for rotating machinery in nuclear power plants based on deep convolutional conditional generative adversarial network. Nuclear Engineering and Technology 2023; 55(6): 2096–2106, https://doi.org/10.1016/j.net.2023.02.036.
46. Wu K, Mei Y. Multi-focus image fusion based on unsupervised learning. Machine Vision and Applications 2022; 33(5): 1–14, https://doi.org/10.1007/s00138-022-01326-6.
47. Xia M, Li T, Xu L, et al. Fault diagnosis for rotating machinery using multiple sensors and convolutional neural networks. IEEE/ASME Transactions on Mechatronics 2018; 23(1): 101–110, https://doi.org/10.1109/TMECH.2017.2728371.
48. Xiao L, Mao Q, Lan P, Zang X, Liao Z. A fault diagnosis method of insulator string based on infrared image feature extraction and probabilistic neural network. 10th International Conference on Intelligent Computation Technology and Automation (ICICTA) 2017; pp. 80–85; https://doi.org/10.1109/ICICTA.2017.25.
49. Xu G, Liu M, Jiang Z, Dirk Söffker D, Shen W. Bearing fault diagnosis method based on deep convolutional neural network and random forest ensemble learning. Sensors 2019; 19(5): 1088, https://doi.org/10.3390/s19051088.
50. Xu J, Zhang Z, Hu X. Extracting semantic knowledge from GANs with unsupervised learning. IEEE Transactions on Pattern Analysis and Machine Intelligence 2023; 45(8): 9654–9668, https://doi.org/10.1109/TPAMI.2023.3262140.
51. Yan H, Bai H, Zhan X, Wu Z, Wen L, Jia X. Combination of VMD mapping MFCC and LSTM : A new acoustic fault diagnosis method of diesel engine. Sensors 2022; 22(21): 8325, https://doi.org/10.3390/s22218325.
52. Yang Y, Zhou Y, Yue X, et al. Real-time detection of crop rows in maize fields based on autonomous extraction of ROI. Expert Systems with Applications 2023; 213(Part A): 118826, https://doi.org/10.1016/j.eswa.2022.118826.
53. Zabihi-hesari A, Ansari-rad S, Shirazi F A. Fault detection and diagnosis of a 12-cylinder trainset diesel engine based on vibration signature analysis and neural network. Proceedings of the Institution of Mechanical Engineers, Part C: Journal of Mechanical Engineering Science

2019; 233(6): 1910–1923, https://doi.org/10.1177/0954406218778313.

54. Zhao H, Zhang J, Jiang Z, Wei D, Zhang X, Mao Z. A new fault diagnosis method for a diesel engine based on an optimized vibration Mel frequency under multiple operation conditions. Sensors 2019; 19(11): 2590, https://doi.org/10.3390/s19112590.
55. Zhao M, Lin J. Health assessment of rotating machinery using a rotary encoder. IEEE Transactions on Industrial Electronics 2018; 65(3): 2548–2556, https://doi.org/10.1109/TIE.2017.2739689.